Anthropogenic Modulation of Dust-Dominated Ice Nucleation in an Urban Dryland City of China during Winter and Spring

Chengqing Chen[1], Yang Wang[1*], Jiming Li[1], Lu Feng[1], Tianrong Chai[1], Zhao Ji[1], Jian Wang[2], Yuan Wang[1]

[1]College of Atmospheric Sciences and Key Laboratory for Semi-Arid Climate Change of the Ministry of Education, Lanzhou University, Lanzhou, 730000, China
[2]Nanjing Handa Environmental Technology Co., Ltd., Nanjing, 211102, China

Correspondence to: Yang Wang (wang_yang@lzu.edu.cn)

Abstract. Ice-nucleating particles (INPs) are crucial for cloud and precipitation modulation~~cloud formation and precipitation~~, yet their variability and sources or properties~~influencing factors~~ in urban dryland regions remain poorly understood. While natural dust is recognized as substantial INPs~~the dominant INP source~~, interactions between dust and anthropogenic pollutants, and how they alter INP abundance remain~~the extent to which anthropogenic pollution modulates INP abundance remains~~ insufficiently quantified. Here, we present online observations of INPs (−15 to −35 °C), together with co-located aerosol size distribution and chemical composition in Lanzhou from winter 2024 to spring 2025. We show that long-range dust transport boosts INP concentrations by ×15 at −30 °C. Elevated secondary inorganic aerosol during pollution in winter was enhanced and negatively correlated with INP activity (R = −0.71). We further refine an INP parameterization based on aerosol size (1–2.5 μm) and freezing temperature, which~~a two-parameter scheme (1–2.5 μm aerosol diameter and temperature) that~~ reproduces 83% of observations within a factor of 5. These findings underscore the need to include local aerosol heterogeneity and dust-pollution interactions in INPs parameterizations for more accurate regional climate simulations.

1. Introduction

Ice-nucleating~~Ice nucleating~~ particles (INPs) significantly reduce the energy barrier for ice crystal formation on water-insoluble aerosol surfaces by inducing heterogeneous nucleation at temperatures above −38°C (Pruppacher et al., 1998; Hoose and Möhler, 2012). Despite their extremely low atmospheric concentrations~~ (typically only 10^{-3} to 10^{-5} of background aerosols)~~, INPs are critical for initiating ice-phase processes that govern cloud phase partitioning (Wang et al., 2015) and precipitation efficiency (Murray et al., 2012; Hawker et al., 2021). Owing to this microphysical sensitivity, cloud-seeding experiments have shown that artificially enhancing INP concentrations in supercooled clouds can shift the timing and spatial distribution of precipitation (French et al., 2018). It has been well established that most terrestrial precipitation originates from ice-phase processes, which are strongly influenced by the abundance and properties of INPs (Field and Heymsfield, 2015; Kärcher, 2022). Therefore, by regulating ice crystal number concentrations, INPs subsequently affect cloud microstructure, lifetime, and radiative properties, thereby contributing to aerosol indirect radiative forcing and posing a major source of

uncertainty in climate modeling (Morrison et al., 2020; Gjelsvik et al., 2025).

INP concentrations commonly span about seven orders of magnitude across the typical temperature range in mixed-phase clouds, and can differ by up to three orders of magnitude even at the same temperature (Petters and Wright, 2015; DeMott et al., 2010). These variations are influenced by multiple factors, including particle source, chemical composition, and surface morphology (Kanji et al., 2017). Mineral dust is considered the abundant~~dominant~~ natural source of INPs in mixed-phase clouds, with East Asian dust being particularly effective due to its relatively high ice-nucleating activity (Chatziparaschos et al., 2023; Kawai et al., 2021). Biogenic particles, such as pollen, bacteria, and fungal spores, can also contribute significantly in warm (> −10°C) and biologically active environments (Pereira Freitas et al., 2023). Marine sea spray aerosols are a major source of INPs in remote oceanic regions (McCluskey et al., 2023). On a global scale, the contribution of biomass burning aerosols (BBAs), mainly emitted by wildfires, to atmospheric INPs remains uncertain and highly variable. Although some field observations report elevated INP concentrations under biomass-burning-influenced conditions (Zhao et al., 2024), this association may partly reflect the presence of co-lofted materials such as mineral dust rather than a direct contribution from BBAs themselves (Chen et al., 2025).~~On a global scale, the concentration of INPs from biomass burning aerosols (BBAs), primarily emitted by wildfires, is substantially higher than that of marine sources (Zhao et al., 2024). Nevertheless, laboratory-based simulations often underestimate INP concentrations from BBAs when compared to field observations (Chen et al., 2025).~~

Urban aerosols, shaped by diverse natural and anthropogenic sources, exhibit complex INPs characteristics: concentrations are strongly influenced by the long-range transport of desert dust (Bi et al., 2019), while black carbon (BC) from anthropogenic emissions generally exhibits low ice-nucleating efficiency under immersion freezing conditions (Kanji et al., 2020). The ice-nucleating efficiency of metal and metal-oxide particles varies strongly with chemical composition, and many pure metals and metal oxides exhibit poor ice-nucleating ability (Yakobi-Hancock et al., 2013); however, metal elements are widely used as tracers of fine mineral dust (Liu et al., 2022) and thus provide useful information on mineral-related contributions to atmospheric INPs. In suburban regions heavily affected by human activity, organic aerosols and anthropogenic dust (e.g., road dust from traffic emissions) have been identified as effective INP sources (Tian et al., 2022; Chen et al., 2024b). Moreover, anthropogenic pollution may influence cloud glaciation processes. Elevated cloud freezing temperatures have been reported under polluted conditions (Pan et al., 2024). INP number concentrations have been observed to differ between clean and polluted environments (Ren et al., 2023)~~Moreover, anthropogenic pollution may increase cloud freezing temperatures (Pan et al., 2024) and enhance the contrast in INP number concentrations under clean versus polluted conditions (Ren et al., 2023)~~. However, some studies report that severe urban pollution does not lead to significant changes in INP concentrations(Chen et al., 2018; Zhang et al., 2022). These conflicting observations highlight the limited understanding of the mechanisms underlying pollution-related INPs variability, further contributing to the uncertainties in INP parameterizations within current climate models (Burrows et al., 2022; Herbert et al., 2025).

Most weather and climate models employ simplified empirical parameterization methods, one of the most representative being the scheme introduced by DeMott et al. (2010), commonly referred to as D10, which is widely integrated into global climate models and high-resolution cloud-resolving~~cloud resolving~~ models (Burrows et al., 2022). As an empirical, size-based

approach, the D10 scheme primarily relates INP number to particles larger than 0.5 μm in diameter~~diameter~~, offering a practical proxy for INP-relevant aerosols. However, it does not explicitly account for mixing-state effects or aerosol compositions as emphasized in Phillips et al. (2008).~~leaving aerosol composition and mixing state effects largely unresolved.~~ This simplification introduces additional uncertainty in polluted environments, where mineral dust-pollution interactions and abundant pollution-derived aerosols may alter INP activity and complicate size-based representations. These challenges are not limited to polluted regions and~~This limitation~~ have~~s~~ motivated recent efforts to develop source-aware parameterizations that explicitly include multiple aerosol types for improved regional applicability of INPs simulations (DeMott et al., 2015; McCluskey et al., 2019).

The stagnant and compositionally complex aerosols in Lanzhou, an inland major city close to the Tibetan Plateau, shaped by its arid climate and enclosed terrain, provide a valuable setting for studying INPs behavior under mixed aerosol regimes (Tan et al., 2017). While winter heating promotes the buildup of fine-particle pollution dominated by organics and secondary inorganics (Du et al., 2020), springtime dust transport and construction activity enhance coarse particle resuspension, leading to a higher contribution from crustal materials (Cheng et al., 2022). Road dust, as a persistent local resuspension source, significantly contributes to $PM_{2.5}$, accounting for up to 51.7% of emissions in developing urban areas (Chen et al., 2019). Concurrently, the rising fraction of organic components in Lanzhou aerosols underscores the influence of traffic emissions and secondary photochemical processes (Xu et al., 2014; Wang et al., 2021). Despite these complex aerosol regimes~~conditions~~, systematic INP observations in the region remain scarce, and hence the applicability of parameterization schemes developed in other environments under such an aerosol regime remains uncertain.

This study focuses on Lanzhou, a typical semi-arid inland city in northwest China, where systematic observations of INPs and concurrent measurements of aerosol physical and chemical properties were conducted during winter and spring. These efforts provide valuable additions to long-term INP datasets under atmospheric conditions affected by both anthropogenic pollution and dust events. Building on these observations, we investigated the inter-seasonal differences of INP concentrations in the urban atmosphere, compared nucleation efficiency across different aerosol pollution events, and developed an empirical parameterization applicable to urban background in Northwest China. This research contributes to a better understanding of INP formation mechanisms in complex source environments and provides theoretical support for improving the parameterization of INP concentrations in regional climate models.

2. Data and Methods

2.1 Overview of field campaign

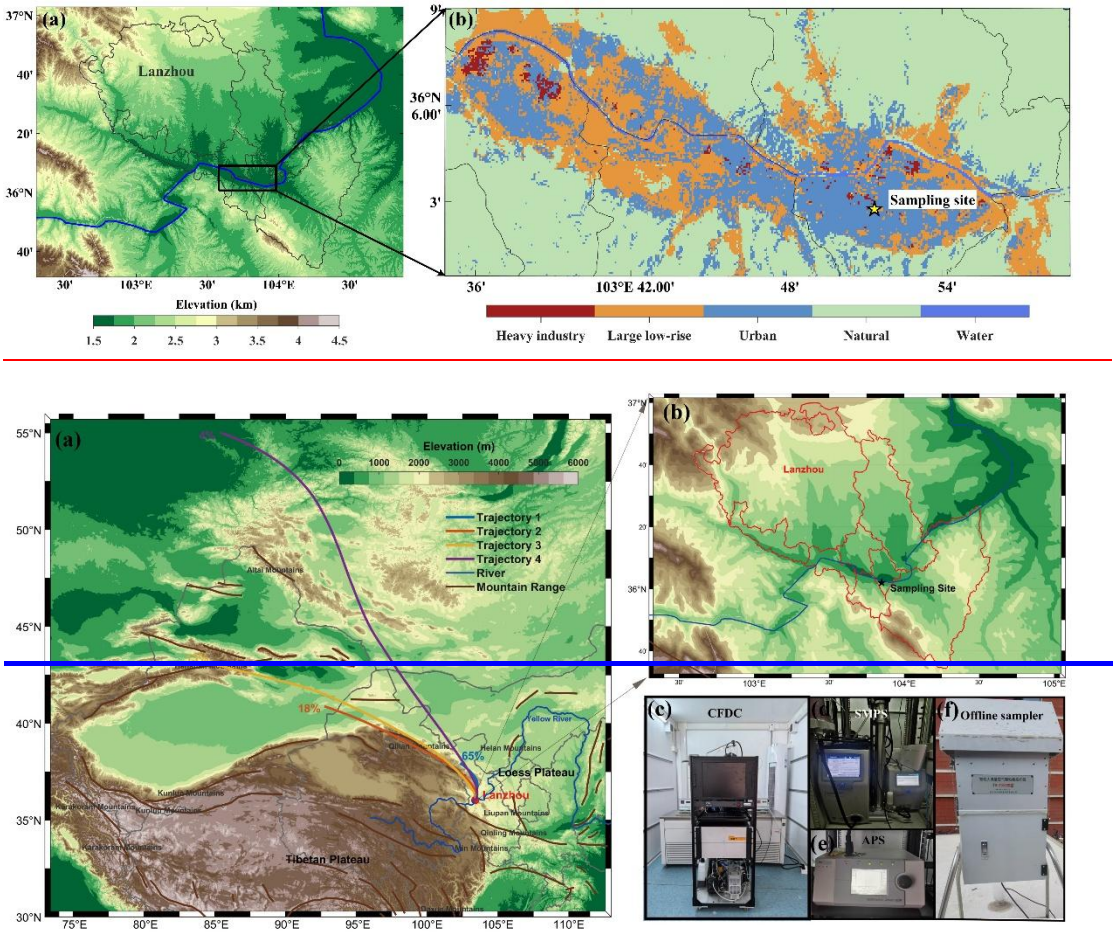

Fig.1. Overview of the location of observations ~~and instrument platform~~. (a) Regional topography of Lanzhou. black box denotes the urban area shown in panel (b). (b) Local-scale Local Climate Zone classification of the Lanzhou urban area, with the sampling site marked by a star.~~(a) Geographical location of Lanzhou City and the air mass transport trajectories. The path represents the result of backward trajectory analysis using the HYSPLIT model over the entire sampling period. (b) Location of sampling site. The red solid line marks the boundary of Lanzhou City, and the altitude is referenced in (a). The black five-pointed star marks the sampling site. (c–f) Photographs of key instruments at the sampling site.~~

This study conducted atmospheric INPs observations during the winter and spring from 12 December 2024 to 21 April 2025. The sampling site was located on the campus of Lanzhou University (103°51′E, 36°2′N, 3m above ground level, AGL) in Lanzhou City, Northwest China, which represents a typical semi-arid inland urban environment (Fig. S1).~~), situated in a typical semi-arid urban background city in Northwest China.~~ Lanzhou is situated in a narrow river valley along the upper reaches of the Yellow River and is surrounded by complex terrain (Fig. 1). This enclosed topographic setting frequently suppresses atmospheric dispersion and favors the accumulation and interaction of aerosols within the urban boundary layer (Chen et al., 2019). As a result, the sampling site is influenced by both regional dust transport and local anthropogenic

activities. Due to the surrounding mountainous terrain, atmospheric pollution is primarily driven by local emissions (65%) and external air mass inputs from various directions (18%, 13%, and 4%, respectively) as shown in Fig. 1, which depicts the relative sources of the air masses in the backward trajectory analysis.

The observation was conducted using a container-type mobile station, where key monitoring parameters, including INP concentration and aerosol particle number size distribution ($N(D)$), and black carbon (BC) mass concentration, were continuously measured. Ambient aerosols were sampled using the same container-based mobile observation system as described in Wang et al. (2025), without an external size-selective inlet. The CFDC instrument is equipped with two size-selective inlets connected in series, and details are provided in Sect. 2.5. Additionally, a National Atmospheric Super Monitoring Station is co-located on the campus and provides supporting measurements of aerosol chemical composition. A detailed description of the monitoring station can be found elsewhere (Du et al., 2020; Li et al., 2023). were measured, and photographs of the instruments are shown in Fig. 1c–e. In addition, A seven-wavelength Aethalometer (AE33, Magee Scientific Inc.) was employed to measure aerosol absorption coefficients and derive equivalent BC mass concentration.

Since the station lacked an online mass concentration monitoring instrument, $PM_{2.5}$ mass concentration data were obtained from the National Environmental Monitoring Station at the Railway Design Institute, located approximately 1.7 km away. Additionally, the National Atmospheric Super Monitoring Station, also located on the campus, provided $PM_{2.5}$ measurements of major water-soluble inorganic ions (NH_4^+, NO_3^-, SO_4^{2-}, Na^+, Mg^{2+}, Ca^{2+}, Cl^-, and K^+) from an online ion chromatograph (IC) and elemental concentrations (e.g., Ca, Al, Fe, Ti, Si) from a heavy-metal analyzer (XHAM-2000), offering essential support for the aerosol composition analysis. In the meantime, an offline particle collection was also conducted using a high-volume sampler and Pall 7204 quartz fiber filters (Fig. 1f).

2.2 Aerosol size distribution measurements

A Scanning Mobility Particle Sizer (SMPS; Model 3082, TSI Inc.) was employed to measure the electrical mobility diameter Stokes diameter (D) in the size range of 13.6 nm to 532.8 nm, divided into 103 bins, with a complete scan conducted every two minutes. The Stokes diameter is denoted as D and is approximately equal to the electrical mobility diameter (Hinds, 1999; Baron and Willeke, 2011). An Aerodynamic Particle Sizer (APS; Model 3321, TSI Inc.) was used to measure the aerodynamic diameter (D_a) in the range of 0.542 to 19.81 umμm, divided into 51 size bins, with a full scan performed every five minutes. To minimize humidity-related measurement errors, which could lead to size overestimation due to particle growth, the particle stream was dried using a silica gel diffusion dryer. The D_a size distribution obtained by the APS was converted to D distribution by assuming an effective particle density of 1.5 g cm^{-3}, a typical value for urban aerosol environments (Zhang et al., 2022), so that the size distributions from different instruments could be merged.

All particle size distribution data were averaged to 10-minute intervals to enable temporal alignment and reduce short-term statistical fluctuations before merging. To reduce instrument noise, the observation data were averaged over 10-minute intervals. This allowed for the merging of the data sizes across instruments (e.g., INP measurement) while reducing statistical fluctuations and enhancing the accuracy of the size distribution. After combining the data from both instruments, several

particle size distribution parameters were calculated, including the $N(D)$, surface area concentration distribution, and volume concentration distribution. The attached diagram (Fig. S2~~1~~) shows the combined particle size results for the entire sampling period, which exhibited no significant biases and acceptable levels of precision.

2.3 Aerosol chemical composition and reconstructed tracers

Aerosol chemical composition data were used to characterize particulate matter properties relevant to INP variability. A seven-wavelength Aethalometer (AE33, Magee Scientific Inc.) was employed to measure aerosol absorption coefficients and derive equivalent BC mass concentration (Wang et al., 2024a). BC mass concentration was measured at a native time resolution of 1 min at 370, 470, 520, 590, 660, 880, and 950 nm. The BC mass concentrations were calculated by the light absorption coefficients at 880 nm (Li et al., 2023) and a 10 min moving average was applied before analysis. In addition, The National Atmospheric Super Monitoring Station, provided $PM_{2.5}$ measurements of major water-soluble inorganic ions (NH_4^+, NO_3^-, SO_4^{2-}, Na^+, Mg^{2+}, Ca^{2+}, Cl^-, and K^+) as mass concentrations ($\mu g\ m^{-3}$) from an online ion chromatograph (IC) and elemental mass concentrations ($\mu g\ m^{-3}$; e.g., Ca, Al, Fe, Ti, Si) from a heavy-metal analyzer (XHAM-2000), offering essential support for the aerosol composition analysis (Tian et al.,2023). Both ion and elemental composition data were recorded at an hourly time resolution.

Reconstructed chemical tracers, including Fine mineral dust (FMD) and secondary inorganic ions (SNA), were derived to represent major aerosol types and processes. To further elucidate the drivers of the observed differences in INP activity among the event types, we focused on −30 °C for detailed analysis, because it is a characteristic temperature at which immersion freezing is most frequently examined ~~(Fig. 6)~~. ~~Fine mineral dust (~~FMD~~)~~ in $PM_{2.5}$ was determined following Malm et al. (1994), and was used as a mineral dust tracer representing both locally resuspended urban dust and transported mineral dust. Specifically, FMD was estimated from the major crustal elements measured in $PM_{2.5}$ using the following mass reconstruction equation:

$$FMD = 2.20\ Al + 2.49\ Si + 1.63\ Ca + 2.42\ Fe + 1.94\ Ti \quad (1)$$

where Al, Si, Ca, Fe, and Ti denote the measured elemental concentrations. The coefficients account for the contribution of associated oxides and represent the typical stoichiometric ratios of aluminosilicate mineral dust.

SNA was quantified as the summed concentration of SO_4^{2-}, NO_3^-, NH_4^+, a commonly used formulation that reflects the overall loading of secondary inorganic aerosol and serves as an indicator of pollution processing (Hu et al., 2017). Specifically, SNA was calculated as:

$$SNA = SO_4^{2-} + NO_3^- + NH_4^+ \quad (2)$$

with all components expressed as $PM_{2.5}$ mass concentrations. It should be noted that these reconstructed tracers are used here as empirical proxies to characterize relative variations in major aerosol components rather than exact mass apportionment.

2.4 Aerosol event categorization

Since the sampling site~~the station~~ lacked an online mass concentration monitoring instrument, hourly $PM_{2.5}$ mass concentration data were obtained from the National Environmental Monitoring Station at the Railway Design Institute, located approximately 1.7 km away. ~~Additionally, the National Atmospheric Super Monitoring Station, also located on the campus, provided $PM_{2.5}$ measurements of major water-soluble inorganic ions (NH_4^+, NO_3^-, SO_4^{2-}, Na^+, Mg^{2+}, Ca^{2+}, Cl^-, and K^+) from an online ion chromatograph (IC) and elemental concentrations (e.g., Ca, Al, Fe, Ti, Si) from a heavy-metal analyzer (XHAM-2000), offering essential support for the aerosol composition analysis.~~To investigate how different aerosol regimes~~conditions~~ influence INP activity, we categorized the observation period into four event types (Fig. S3~~6~~). Dust events were identified by $PM_{10} \geq 150$ μg m^{-3}, while non-dust conditions were further separated into Clean, Moderate, and $PM_{2.5}$ High categories according to $PM_{2.5}$ thresholds of 35 and 75 μg m^{-3}. The PM_{10} can effectively capture the arrival of dust intrusions and has been used in previous studies to identify periods of coarse-mode aerosol enhancement (Lei et al., 2014; Wang et al., 2024b), while $PM_{2.5}$ serves as a useful indicator of pollution severity (Ren et al., 2023). In combination, these two indicators offer a representative and widely comparable basis for separating dust events from varying levels of pollution. The occurrence frequencies and INP characteristics associated with the different aerosol event types are presented in Sect. 3.2.

2.5~~3~~ INPs observations

INP measurements in this study were performed using a commercial Continuous Flow Diffusion Chamber–Ice Activation Spectrometer (CFDC-IAS), which is based on the well-established CSU-CFDC design (Rogers et al., 2001; DeMott et al., 2015) and is capable of autonomous operation with minimal in-person handling and full remote access (Bi et al., 2019). Hereafter, this instrument is referred to as CFDC.~~The INPs measurement used in this study is a new type of Continuous Flow Diffusion Chamber-Ice Activation Spectrometer (CFDC-IAS), hereafter referred to as CFDC, capable of autonomous operation with minimal in-person handling and full remote access.~~ Detailed technical specifications and theoretical descriptions have been comprehensively documented in previous instrument publications (Lacher et al., 2024; DeMott et al., 2017, 2025). The chamber comprises ~~consists of~~ two concentric cylindrical walls, each maintained at different temperatures through an ethanol circulation system. The inner surfaces are coated with ice, creating a temperature and humidity gradient in the upper growth region of simulated cloud particles, where aerosol particles activate, nucleate, and grow as ice crystals.~~ This gradient activates the aerosol particles, leading them to nucleate into ice crystals and grow.~~ In the lower evaporation region, liquid droplets~~ are~~ rapidly evaporate~~d~~, leav~~ensur~~ing ~~that~~ only ~~solid~~ ice crystals for~~remain when particles larger than 3 μm are detected by the~~ optical particle counter (OPC) detection. The sheath gas flow rate and sample flow rate were set at 7.5 L min^{-1} and 1.5 L min^{-1}, respectively, to ensure stable delivery of both the gas flow and sample. ~~Water supersaturation conditions (typically 104% 106% RH_w, where RH_w denotes relative humidity with respect to liquid water) were maintained in the growth area, forcing aerosols to first activate into cloud droplets before undergoing ice nucleation, yielding results similar to the offline immersion freezing technique (Moore et al., 2024).~~ Water supersaturation conditions (typically 4–6% SS_w), consistent with those reported by Moore et al. (2024) for immersion freezing, were maintained in the growth section. Here, SS_w denotes

supersaturation with respect to liquid water and is defined as $SS_w = RH_w - 100\%$.

Before the experimental observations, the performance of the CFDC was assessed~~the performance of the CFDC was verified through calibration~~ using ammonium sulfate and illite-NX under representative temperature and supersaturation conditions (Fig. S4~~2~~–S5~~3~~). These tests were intended to verify stable OPC-based ice crystal detection and chamber operation under immersion-freezing conditions. Illite-NX and ammonium sulfate are standard reference materials widely used in CSU-CFDC studies to characterize heterogeneous and homogeneous freezing (Richardson et al., 2010; Hiranuma et al.,2015). The thermodynamic freezing onset characteristics of these materials have been systematically documented for the standard CSU-CFDC configuration over comparable temperature and supersaturation ranges (e.g., Rogers et al., 2001; Kanji et al., 2011; Levin et al., 2014). To ensure accurate measurements, the aerosol stream was dried below the frost point using silica gel and molecular sieves. Aerosol particles that could interfere with the optical detection of ice crystals were removed by passing the aerosol stream through two identical single-jet impactors in series (D50 = 2.5 µm), where D50 denotes the aerodynamic particle diameter at which 50% of particles are transmitted through the impactor. ~~Aerosol particles larger than 3 µm, which could interfere with the optical detection of ice crystals, were removed by passing the aerosol stream through two identical single-jet impactors (cut size = 2.5 µm) in series.~~ The CFDC is serviced weekly, with the diffusion desiccant replaced, O-rings sealed, the water tank replaced when necessary, and the nitrogen tank changed as needed. The experimental temperature ranged from −15°C to −35°C, with a 5°C interval, to fully investigate ice nucleation activity under varying temperature conditions. The measurement cycle was 5 minutes, alternating with a 5-minute HEPA-filtered air cycle to provide background counts for the instrument. During this process, the INP concentration was background-corrected using data from the adjacent filtered air cycle (Barry et al., 2021). The effective detection limit of the CFDC is not a fixed instrumental constant but depends, for example, on the sampling flow rate, integration time, and background ice counts (Demott et al., 2017). Under the operating conditions applied here, the effective lower detection limit is estimated to be ~0.13 INP sL^{-1}. In this study, INPs and $N(D)$ results are reported under standard conditions (STP: 0°C, 101.325 kPa).

To ensure temporal consistency across datasets, all aerosol measurements, including $N(D)$, particle mass concentration, BC, and aerosol chemical composition, were temporally matched to INP observations using the same nearest-neighbor approach. For each INP measurement, the closest-in-time data point from each aerosol dataset was selected, provided that the time difference did not exceed 30 min. This time window was chosen to avoid using aerosol data that are temporally too distant from the corresponding INP measurements.

2.64 Back trajectory models

Backward air-mass trajectories were calculated using the Hybrid Single-Particle Lagrangian Integrated Trajectory model (HYSPLIT), developed by the National Oceanic and Atmospheric Administration (NOAA) Air Resources Laboratory (Hofer et al., 2024). The model was driven by the GDAS 1° × 1° meteorological dataset. To determine an appropriate arrival height for trajectory analysis over the entire sampling period, 72 h backward trajectories were first calculated at 1 h intervals for four arrival heights (100, 500, 1000, and 1500 m AGL). The backward trajectory frequency patterns show broadly similar dominant

source regions across the four starting heights, with air masses mainly originating from western and northwestern continental regions (Fig. S6). Despite these differences, the associated land-cover fractions remain relatively consistent among heights. We therefore focus on trajectories arriving at 100 m AGL in the following analyses as representative of near-surface air masses influencing the INP measurements. ~~For each INP measurement, a 72 h backward trajectory was initialized at the sampling site in Lanzhou at an arrival height of 100 m above ground level. The start time of each trajectory was set to the nearest hour preceding the corresponding INP sample to ensure temporal consistency between air mass history and observed aerosol conditions.~~ The resulting trajectories were then used to infer the potential influence of regional dust sources and anthropogenic pollution on the observed INP variability. This approach is commonly applied in field-based INP studies to provide source-context information complementary to in situ aerosol chemical measurements.

The land cover types were obtained from the MODIS Land Cover Type product (MCD12C1 v061) for the year 2024, based on the International Geosphere–Biosphere Programme (IGBP) classification scheme at a spatial resolution of 0.05°. The original 17 IGBP classes were further aggregated into seven major land-cover categories (barren, grass and shrubland, cropland, forest, urban, water and wetland, and snow and ice). To further characterize the underlying surface types along transport pathways, each trajectory was overlaid with a gridded land-cover dataset, and the fractional contributions of major land-cover classes were calculated. This combined trajectory–land-cover analysis is commonly applied in field-based INP studies as a complement to in situ aerosol chemical measurements (Chen et al., 2024a).

3. Results and Discussion

3.1 Dust predominates over pollution in INP bursts

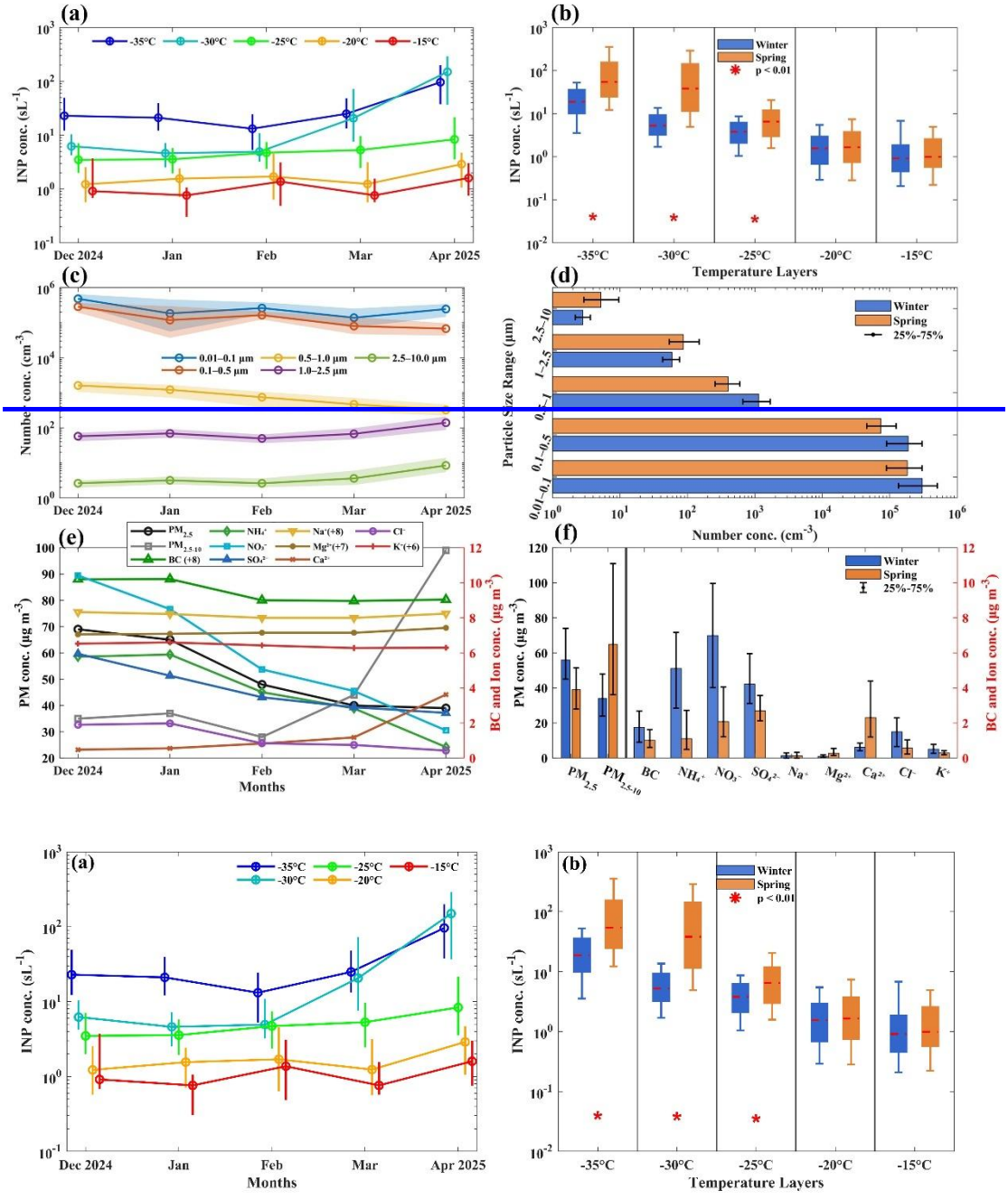

Fig. 2. Monthly variations and Seasonal differences in INPs ~~and related aerosol characteristics~~. (a) Monthly median INP concentrations. (b) Seasonal box plots of INP concentrations in winter (December–February) and spring (March–April); boxes indicate the interquartile range, whiskers the 10th–90th percentiles, and red asterisks denote significant differences. ~~(c) Monthly median aerosol number concentrations in five size bins. (d) Seasonal median aerosol number size distributions. (e) Monthly median mass concentrations. Values in parentheses denote the offsets applied for graphical clarity and actual concentrations should be obtained by subtracting the offset values. (f)~~

~~Seasonal mass concentrations of the same species as in (e). Unless otherwise noted, error bars and shaded areas represent the 25th–75th percentile ranges.~~

In most months and in both seasons, the median INP concentrations decreased as the activation temperature increased from −15 °C to −35 °C (Fig. 2), reflecting the expected temperature dependence of immersion freezing. From December to April, INP concentrations at −15 °C and −20 °C remained relatively stable. In contrast, INPs at −25 °C, −30 °C, and −35 °C showed little variation from December to February, followed by a pronounced increase in March that persisted through April. Over the same period, coarse-mode aerosol (1 μm < D < 2.5 μm) number concentrations showed a similar increase. In addition, mass concentrations of water-soluble mineral-related ions, such as Ca^{2+}, and crustal trace metals were also higher during this period (Fig. S7; Table S1). ~~From February to April, INPs at −25 °C, −30 °C, and −35 °C increased progressively, accompanied by higher coarse-mode aerosol (1 μm < D < 2.5 μm) number concentrations and mineral ions mass concentrations (e.g., Ca^{2+}).~~ This linkage suggests that the seasonal rise in INPs was closely tied to the intensification of the coarse mineral-dust component during spring.

Seasonal comparisons further confirmed the significance of these differences: spring INP concentrations were a factor of 1.4–2.2 higher than winter levels (Mann–Whitney U test; Fig. 2b).~~,~~ These increases coincided~~coinciding~~ with enhanced~~increased~~ coarse-mode aerosol and Ca^{2+}~~$^{2+}$~~, as well as elevated crustal trace metals (Table S1), whereas $PM_{2.5}$, BC, ~~secondary inorganic ions (~~SO_4^{2-}, NO_3^-, NH_4^+~~)~~, and Cl^- were all higher in winter (Fig. S7~~Fig. 2d, 2f~~). Overall, these results indicate a clear redistribution in aerosol composition, with coarse dust dominating in spring and fine particle pollution prevailing in winter, consistent with the enhanced heating-related coal combustion in northwestern China (Du et al., 2020). Such shifts in the dominant aerosol sources are often the main driver of seasonal variations in INPs (Creamean et al., 2022), explaining the substantially higher cold-temperature INP activity observed during spring.

Indeed, a Spring dust intrusion coincided with enhanced coarse-mode aerosol, PM_{10}~~-~~, FMD, and Ca^{2+}, accompanied by a pronounced increase in INP concentrations at −25 °C, −30 °C, and −35 °C (Fig. ~~S4~~S8). Such behavior reflects the high immersion-freezing efficiency of mineral dust, particularly its abundance in the coarse mode during dust intrusions. In contrast, the wintertime $PM_{2.5}$ pollution episode during the Lantern Festival showed no marked change in INP concentrations at most activation temperatures, with only fluctuations observed at −35 °C. This indicates that pollution-derived fine particles, although abundant in winter, have intrinsically low immersion-freezing ability and exert only a minor influence on INPs compared with mineral dust. As meteorological parameters were generally stable (Fig. ~~S5~~S9) and INPs were measured under fixed temperature and humidity conditions, the observed variability was predominantly driven by aerosol influences rather than changes in meteorological conditions. To summarize, the springtime predominance of coarse dust, overriding the wintertime $PM_{2.5}$ pollution, establishes the requisite conditions for the episodic INP bursts (i.e., episodic and pronounced increases in INP concentrations) that characterize the ice nucleation regime in the inland basin.

3.2 INP Characteristics under Different Aerosol Events

~~To investigate how different aerosol conditions influence INP activity, we categorized the observation period into four event types (Fig. S6). The PM_{10} can effectively capture the arrival of dust intrusions and has been used in previous studies to identify periods of coarse-mode aerosol enhancement (Lei et al., 2014), while $PM_{2.5}$ serves as a useful indicator of pollution severity (Ren et al., 2023). In combination, these two indicators offer a representative and widely comparable basis for separating dust events from varying levels of pollution.~~

~~These categories exhibited clear seasonal patterns, with Dust and Clean events occurring mainly in spring, while $PM_{2.5}$ High events were concentrated in winter (Fig. S7).~~ The observations are categorized into four aerosol event types (Clean, Moderate, PM2.5 High, and Dust). These event types e exhibit distinct seasonal preferences, with Dust and Clean events occurring mainly in spring, while PM2.5 High events are predominantly observed in winter (Fig. S10). T~~Moreover, t~~he four categories showed distinct physicochemical characteristics, further confirming the representativeness of this classification (Fig. 3a–3c). Dust events were characterized by markedly high PM_{10} levels and a low $PM_{2.5}/PM_{10}$ ratio (~0.25), indicative of the coarse-mode particles' dominance (Yu et al., 2024). In contrast, $PM_{2.5}$ High events show elevated $PM_{2.5}$ concentrations and higher ratios (0.5–1.0). This divergence was further unequivocally reflected in $N(D)$ (Fig. 3b). Dust events uniquely exhibit a pronounced coarse-mode aerosol concentration with enhanced number concentrations in the $0.5 < D < 1.0$ ~~μm~~μm range, indicative of mineral dust input. Finally, chemical composition indicators, including major ions, BC, and FMD, ~~, the ion composition~~ provided conclusive evidence for distinct particle sources (Fig. 3c). Dust events were marked by abundant mineral ions, whereas $PM_{2.5}$ High events were enriched with BC and secondary inorganic ions, along with additional fine-mode species such as Cl^- and K^+. Moderate events displayed mixed ion characteristics, with concentrations falling between conditions of Dust and $PM_{2.5}$ High events, and Clean events consistently registered the lowest ion concentrations across all species.

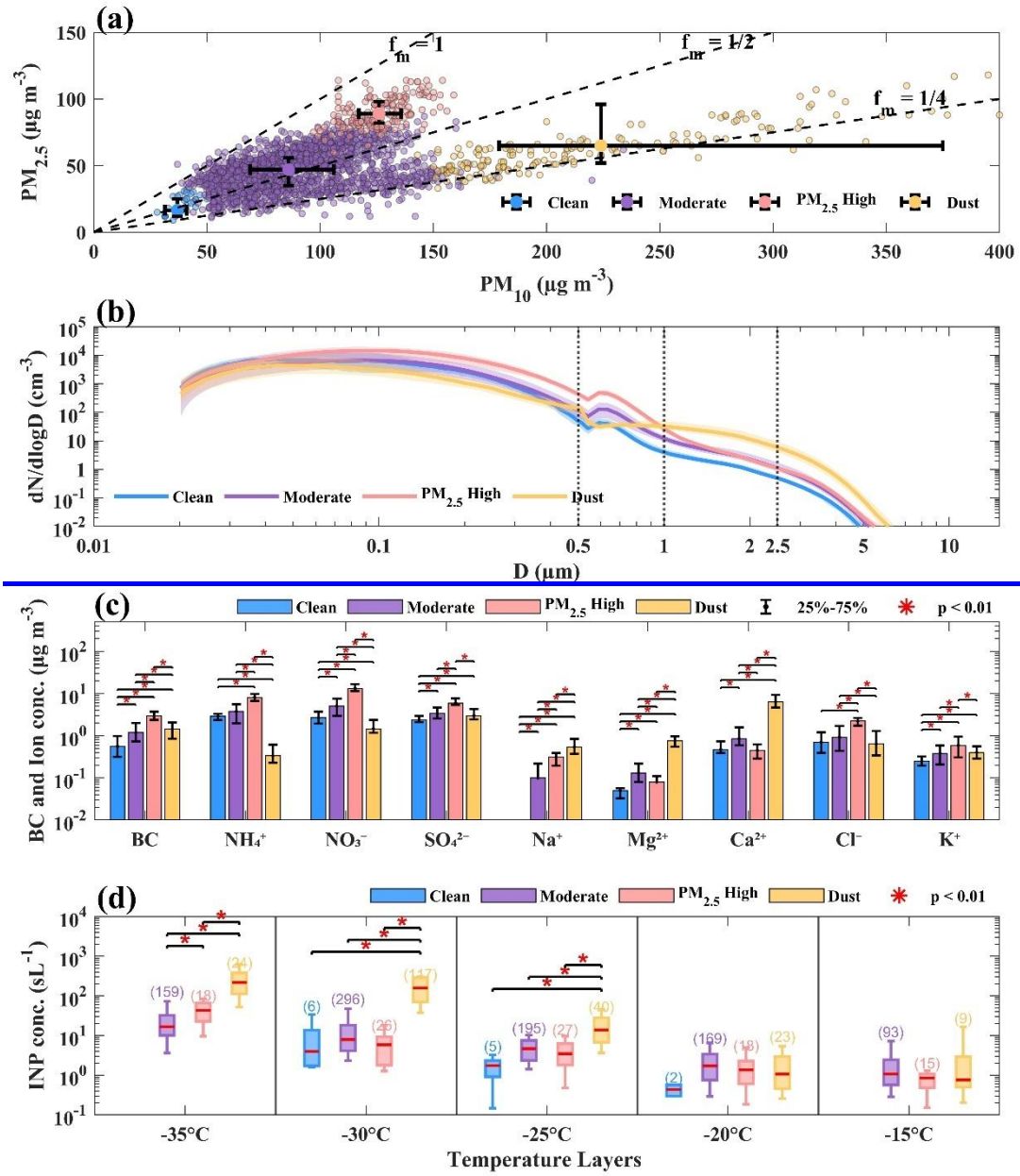
(a)
$f_m = 1$
$f_m = 1/2$
$f_m = 1/4$
Clean
Moderate
$PM_{2.5}$ High
Dust
$PM_{2.5}$ ($\mu g\ m^{-3}$)
PM_{10} ($\mu g\ m^{-3}$)
(b)
dN/dlogD (cm^{-3})
D (μm)
(c)
25%-75%
p < 0.01
BC and Ion conc. ($\mu g\ m^{-3}$)
BC
NH_4^+
NO_3^-
SO_4^{2-}
Na^+
Mg^{2+}
Ca^{2+}
Cl^-
K^+
(d)
INP conc. (sL^{-1})
-35°C
-30°C
-25°C
-20°C
-15°C
Temperature Layers

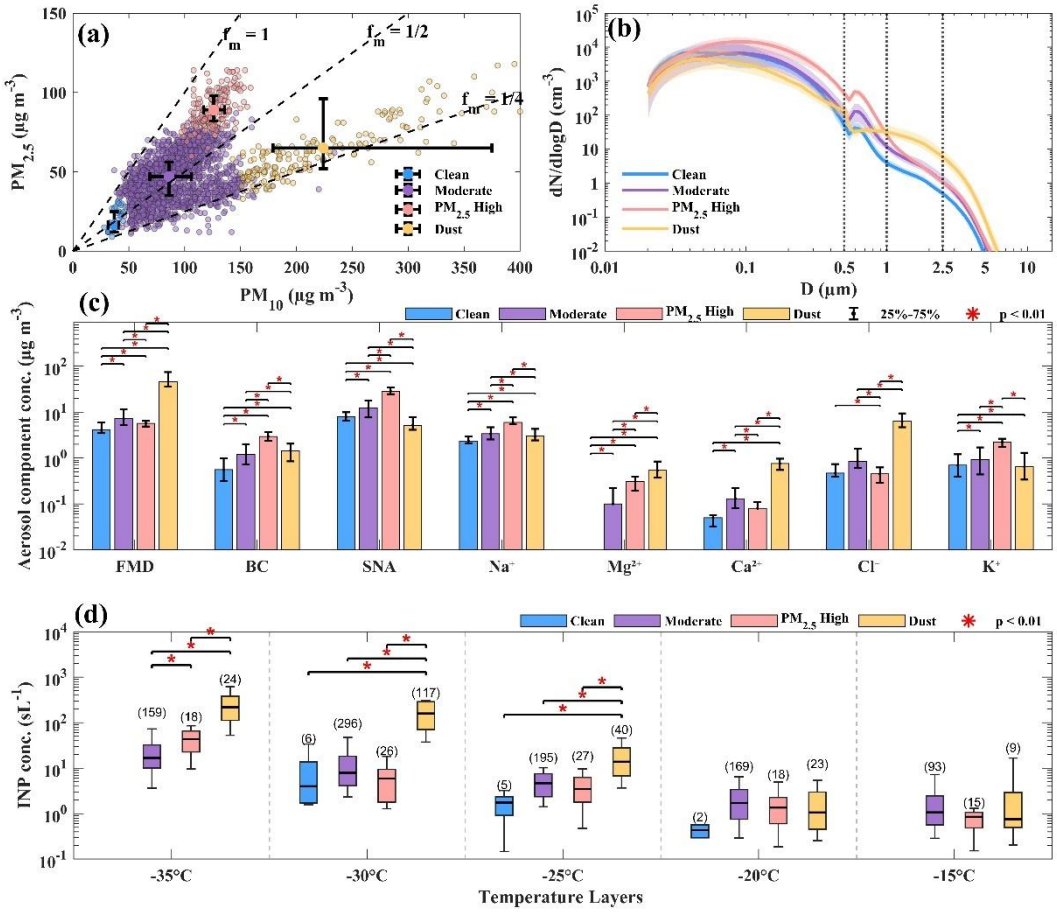

Fig. 3. Comparative analysis of physicochemical characteristics and INP concentrations across different aerosol event types. (a) Mass concentrations of $PM_{2.5}$ and PM_{10}. Solid markers indicate the median, error bars represent the 25th and 75th percentiles, and dashed lines show the $PM_{2.5}/PM_{10}$ ratio (f_m). (b) Particle number size distribution. The solid line indicates the median, and the gray shading represents the 25th–75th percentile range. (c) Mass concentrations of water-soluble ions, shown as median values for different event types. (d) INP concentrations at different temperatures. Boxes represent the 25th–75th percentiles, red lines inside the boxes indicate the median, and whiskers extend to the 10th and 90th percentiles. Numbers in brackets indicate the number of samples corresponding to combinations of aerosol event types and temperature layers~~. (c–d)~~., R~~r~~ed asterisks above the brackets indicate significant differences ($p < 0.01$) between groups based on median tests.

A stark temperature-dependent contrast in INP activity was observed between dust and pollution events (Fig. 3d). INP concentrations in $PM_{2.5}$ High and Moderate events were similar above −30 °C, indicating that pollution-derived fine particles exert limited freezing influence under these conditions. In contrast, dust events diverged sharply at colder temperatures: at −30 °C, INP concentrations during dust events were 15.2 times higher than in Moderate events, and the enhancement further amplified at −35 °C. This strong temperature sensitivity reflects the well-established efficiency of mineral-dust particles in

supplying abundant immersion-freezing-active sites. Notably, A significant divergence emerged only at −35 °C, where fine particles in $PM_{2.5}$ High events also showed significant ice-nucleating ability at −35 °C, implying that small particles can still contain active ice-nucleating sites for ice formation at very low temperatures (Zhao et al., 2019; Tian et al., 2022~~Bertozzi et al., 2021~~). Nevertheless, their activity remained substantially weaker than that of dust aerosols. As expected, Clean events consistently exhibited the lowest INP concentrations across all temperatures, aligning with the overall low aerosol loading and reduced abundance of coarse-mode particles~~the weak ice-nucleating activity in clean atmospheric conditions~~. The coherent ordering of the four event types across activation temperatures highlights the strong modulating influence of aerosol source and size distribution on INP activity.

To compare the ice-nucleating activity among aerosol types, activity parameters normalized by particle number ($N_{D>0.5}$, $N_{D>1.0}$) and ~~,~~ surface area (N_S)~~, and volume (N_V)~~ were calculated (definitions in Appendix Text S1). Dust events consistently exhibit the highest activation fractions and site densities at −25 °C and below, confirming their strong nucleation efficiency of mineral dust particles (Fig. 4~~5~~). Conversely, $PM_{2.5}$ High events displayed the weakest activity from −15 to −30 °C, consistently lower than Moderate and Clean events, yet showed a marked increase at −35 °C, indicating enhanced nucleation potential only under the coldest conditions and likely a very low threshold temperature for appreciable nucleation by $PM_{2.5}$ pollution particles. The consistent pattern across all normalization approaches demonstrates that dust was the dominant ice-nucleating aerosol type during the observation period, particularly in spring.~~ Together, the trajectory and activity analyses confirm that the springtime INP bursts are driven by the long-range import of coarse dust particles, which possess an ice-nucleating efficiency far exceeding that of locally produced $PM_{2.5}$ pollution.~~

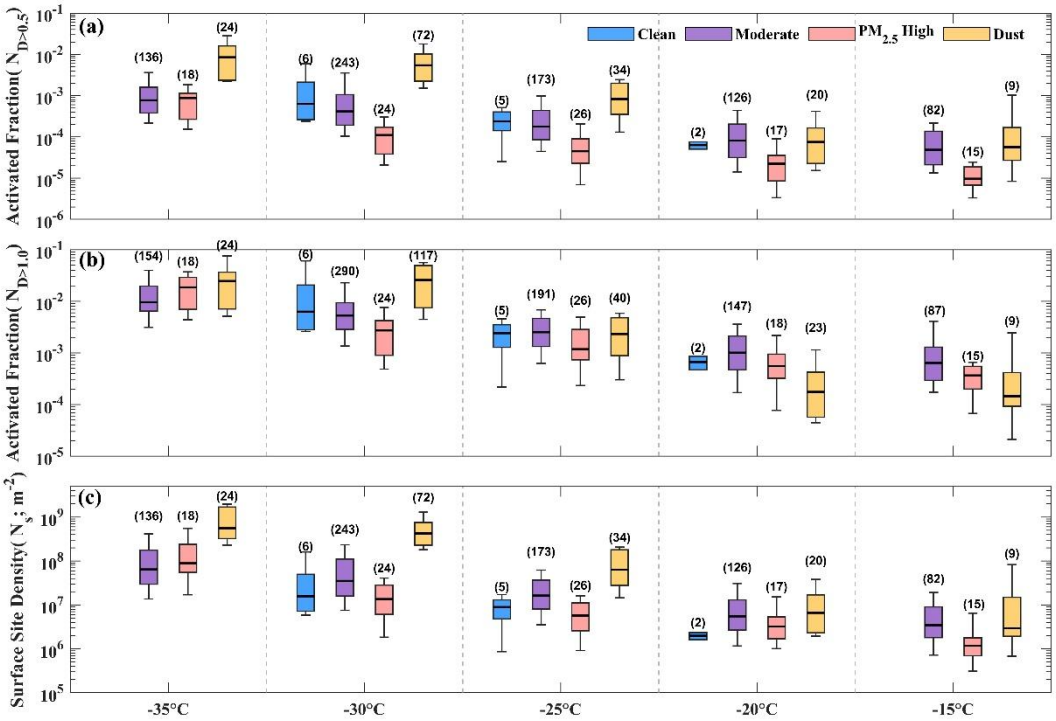

345

Fig. 4. Distributions of ice nucleation activity parameters. Each box shows the 25th–75th percentile range, with the center line indicating the median and the whiskers extending to the 10th and 90th percentiles. Numbers above the boxes indicate the number of samples for each event type at each temperature.

3.3 Backward trajectory and source region analysis

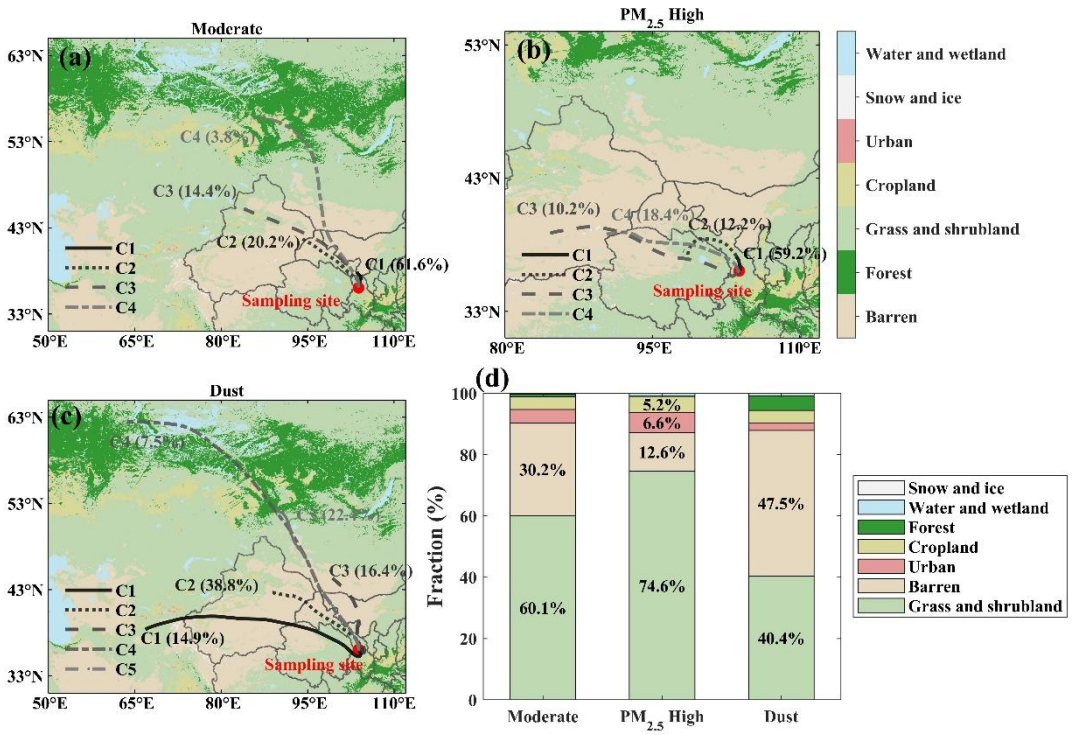

Fig. 5. Spatial distributions of 72-h backward air-mass trajectories and associated land-cover characteristics for different aerosol event events. Panels (a–c) show clustered backward trajectories for (a) Moderate, (b) $PM_{2.5}$ High, and (c) Dust events, overlaid on MODIS land-cover data. The red star indicates the sampling site, and the percentages denote the fraction of trajectories in each cluster. Panel (d) shows the fractional contributions of major land-cover types sampled by trajectories for each event type. Land-cover categories include barren, forest, grass and shrubland, cropland, urban, snow and ice, and water and wetland.

To place the observed contrasts in INP activity into a transport context, we examined air-mass pathways and potential source regions using 72-h HYSPLIT backward trajectory clustering combined with land-cover statistics along the transport pathways (Fig. 5). Dust events were characterized by a pronounced shift toward long-range transport, with clusters C2 (38.8%) and C5 (22.4%) accounting for more than 60% of all trajectories. These trajectories predominantly originated from northwestern inland Asia and frequently crossed extensive desert and semi-arid regions before reaching Lanzhou. Correspondingly, land-cover analysis shows a substantially higher fraction of barren surfaces (47.5%) along Dust trajectories, together with a reduced contribution from grassland and shrubland (40.4%). This coherent pattern between long-range transport pathways and enhanced traversal of arid land surfaces highlights the distinct upstream environments associated with Dust events. Furthermore, near-surface wind fields and synoptic-scale meteorological processes may also modulate INP observations. Existing research indicates that dust events in mid-latitude regions often co-occur with convective systems, gusty winds, and precipitation processes, which can simultaneously influence dust transport, removal, and resuspension of surface sediments (Rivera Rivera et al., 2008). Although this study did not quantitatively analyze the relevant weather processes, under

the Dust scenario, the long-range transport characteristics indicated by the trajectory and the significant increase in the proportion of bare ground surface are consistent with the enhanced performance of INP in the low-temperature segment, and synoptic-scale processes may play a further modulating role.

In contrast, during $PM_{2.5}$ High events, the trajectories were dominated by short-range clusters with limited horizontal displacement (C1: 59.2%), with most air masses remaining within the broader vicinity of Lanzhou. Consistent with this transport pattern, the associated trajectories predominantly traversed grassland and shrubland surfaces (74.6%), with relatively minor contributions from barren land (12.6%) and other land-cover types, indicating that air masses during $PM_{2.5}$ High events were largely confined to near-regional environments rather than originating from remote arid source regions. Moderate events exhibited intermediate transport characteristics, with trajectories distributed among near-regional and regional-scale clusters (C1: 61.6%; C2: 20.2%; C3: 14.4%). The associated land-cover composition was likewise transitional, with trajectories sampling both grassland/shrubland (60.1%) and barren land (30.2%), reflecting a mixture of regional background air masses and episodic inputs from drier source areas. Owing to the limited number of Clean events, trajectory clustering was not performed; backward trajectories for Clean conditions are shown in Fig. S11, and they generally indicate short-range transport within northwestern China. Overall, significant differences in transport path length and the types of land surfaces traversed provide direct transport-level evidence for contrasting INP concentration levels and temperature dependence between Dust and $PM_{2.5}$ High scenarios.~~The 72-h backward trajectory analysis revealed distinct source regions for different event types (Fig. 4). During $PM_{2.5}$ High events, the trajectories were short and exhibited limited horizontal displacement, remaining largely within the broader vicinity of Lanzhou. Such weak transport patterns suggest reduced ventilation residence of air masses in the region, conditions that commonly accompany wintertime fine particle pollution episodes. In contrast, Dust events were linked to long-range transport from exogenous desert and semi-arid regions in northern inland Asia, including southern Siberia, Mongolia, and parts of Central Asia. These trajectories frequently descended from higher altitudes and traversed known dust source regions before reaching Lanzhou, matching previously documented springtime dust transport pathways into northwestern China (Tang et al., 2018). Moderate and Clean events showed shorter and more variable trajectories, often originating from regions within northwestern China. These patterns indicate that the air masses associated with these events underwent relatively limited upwind transport before arriving in Lanzhou. Overall, the trajectory differences delineate the distinct air mass transport histories associated with each event type, providing the relevant transport context for interpreting the observed aerosol and INP characteristics.~~

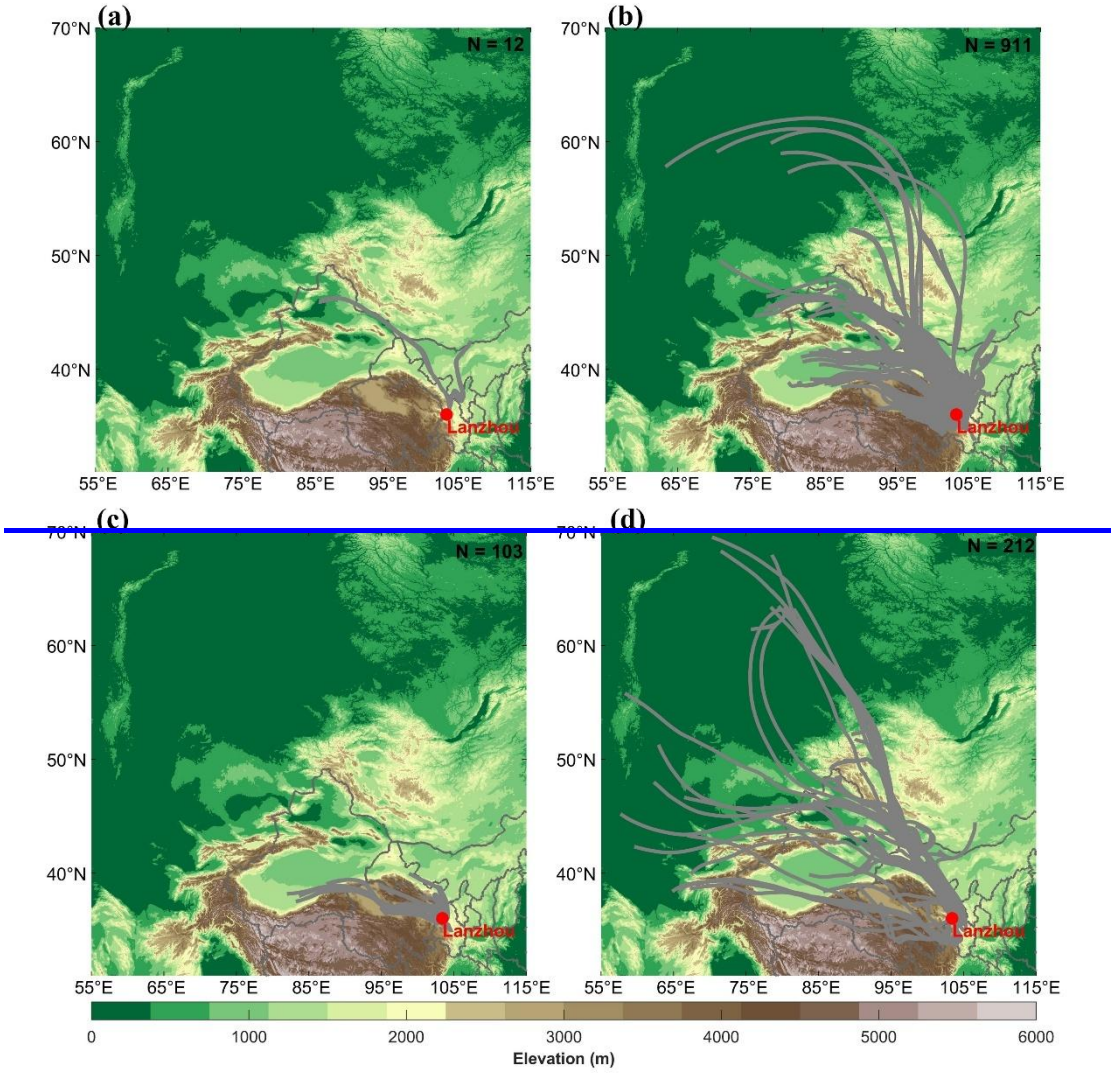

395

Fig. 4. 72 hour backward trajectory distribution of different aerosol event types. (a) Clean events. (b) Moderate events. (c) $PM_{2.5}$ High events. (b) Dust events. The gray curve shows a single backward trajectory for the event type, with the starting point located at an altitude of 100 m at the sampling site. The number of trajectories (N) for the event type is shown in the upper right corner.

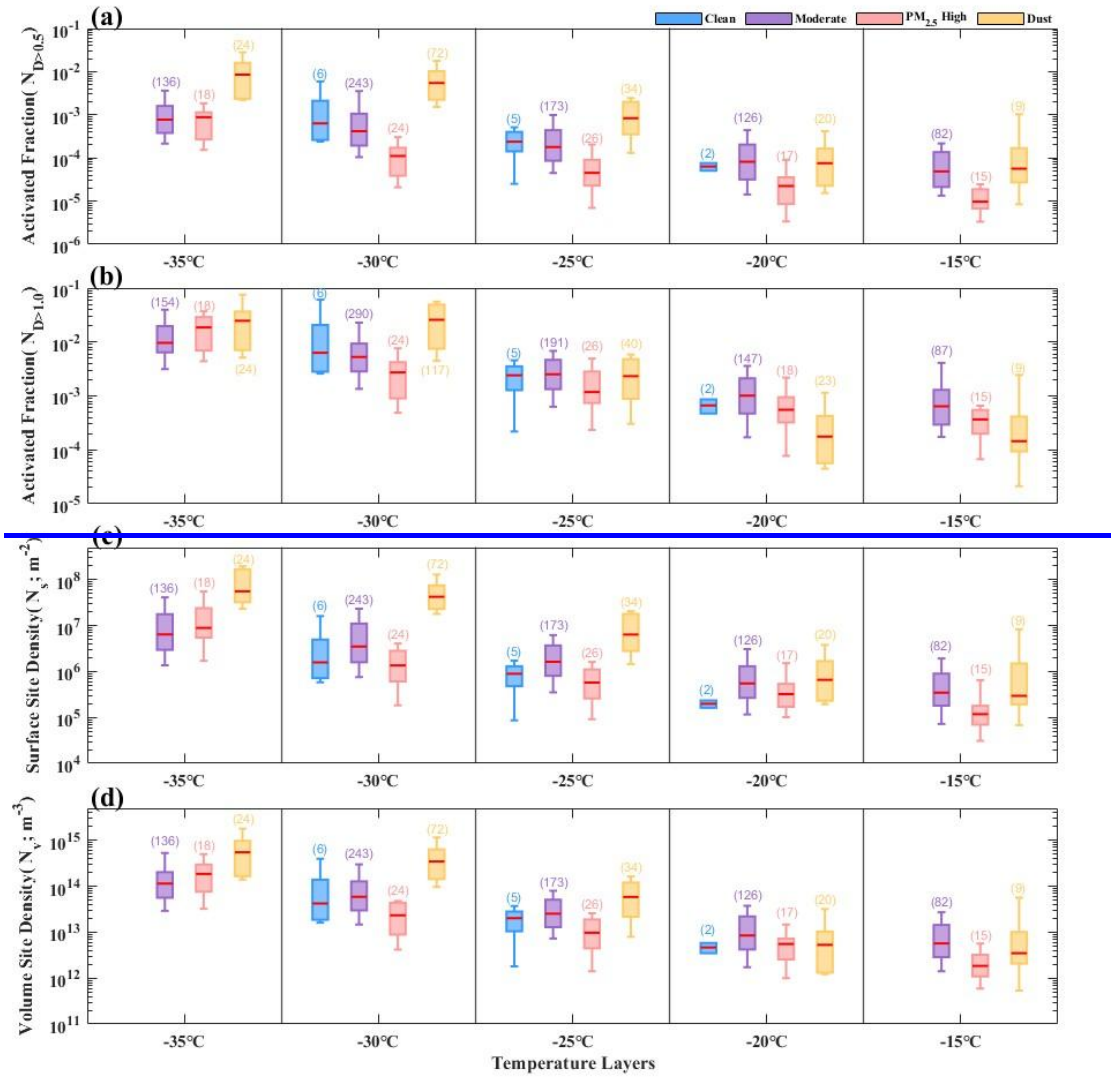

Fig. 5. Distributions of ice nucleation activity parameters. Each box shows the 25th–75th percentile range, with the center line indicating the median and the whiskers extending to the 10th and 90th percentiles. Numbers above the boxes indicate the number of samples for each event type at each temperature.

To compare the ice-nucleating activity among aerosol types, activity parameters normalized by particle number ($N_{D>0.5}$, $N_{D>1.0}$), surface area (N_s), and volume (N_v) were calculated (definitions in Appendix Text S1). Dust events consistently exhibit the highest activation fractions and site densities at −25 °C and below, confirming their strong nucleation efficiency of mineral dust particles (Fig. 5). Conversely, $PM_{2.5}$ High events displayed the weakest activity from −15 to −30 °C, consistently lower than Moderate and Clean events, yet showed a marked increase at −35 °C, indicating enhanced nucleation potential only under the coldest conditions and likely a very low threshold temperature for appreciable nucleation by $PM_{2.5}$ pollution particles. The

~~consistent pattern across all normalization approaches demonstrates that dust was the dominant ice-nucleating aerosol type during the observation period, particularly in spring. Together, the trajectory and activity analyses confirm that the springtime INP bursts are driven by the long-range import of coarse dust particles, which possess an ice-nucleating efficiency far exceeding that of locally produced $PM_{2.5}$ pollution.~~

3.43 Contrasting correlations of dust and SNA with INP activity

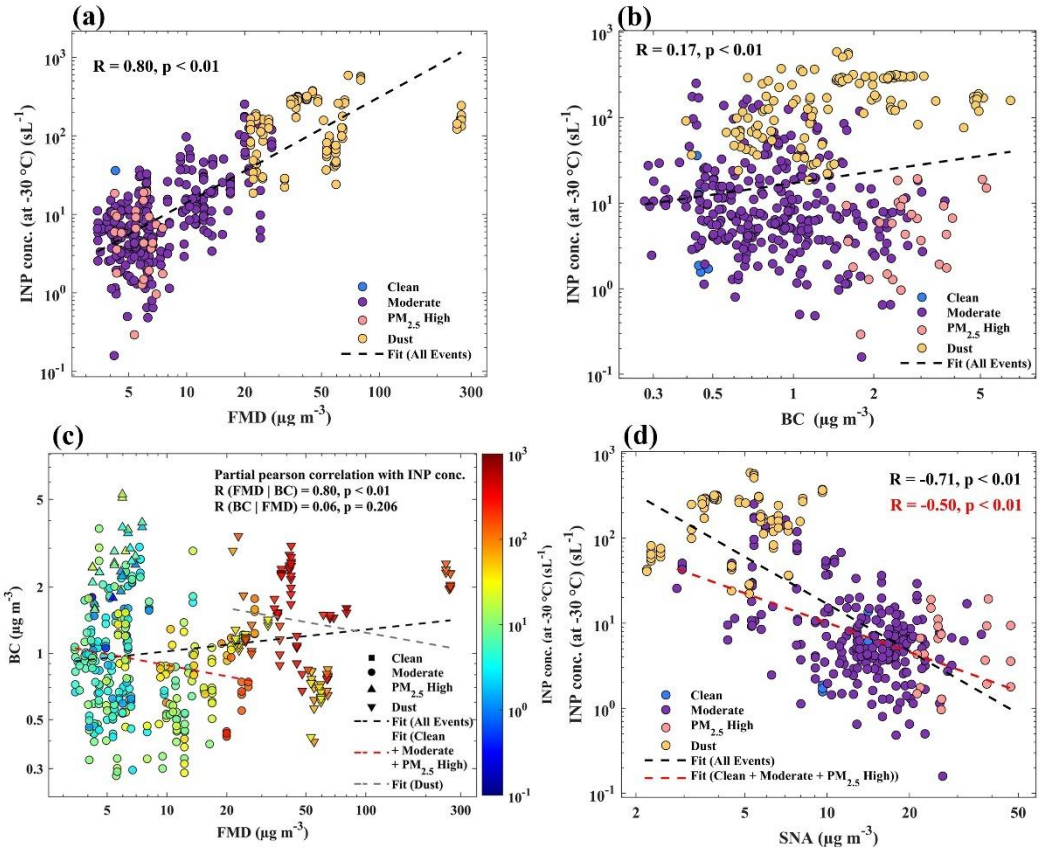

Fig. 6. Associations between -30 °C INP concentrations and aerosol ion components. (a), (b), (d) Scatter plots of INP concentrations versus FMD, BC and SNA mass concentrations, respectively. *R* denotes the Pearson correlation coefficient, and *p* denotes the significance level, calculated in the natural log space. (c) Bivariate plots with FPMD and BC on the axes, where the color scale represents INPs. *R* and *p* denote the partial correlation coefficient and significance level, also calculated in the natural log space.

~~To further elucidate the drivers of the observed differences in INP activity among the event types, we focused on −30 °C for detailed analysis, because it is a characteristic temperature at which immersion freezing is most frequently examined (Fig. 6). Fine mineral dust (FMD) in $PM_{2.5}$ was determined following Malm et al. (1994), and was used as a mineral dust tracer~~

~~representing both locally resuspended urban dust and transported mineral dust. Specifically, FMD was estimated from the major crustal elements measured in $PM_{2.5}$ using the following mass reconstruction equation:~~

To further elucidate the drivers of the observed differences in INP activity among the event types, we focused on −30 °C for detailed analysis, because it is a characteristic temperature at which immersion freezing is most frequently examined (Fig.6). ~~where Al, Si, Ca, Fe, and Ti denote the measured elemental concentrations. The coefficients account for the contribution of associated oxides and represent the typical stoichiometric ratios of aluminosilicate mineral dust.~~ INPs increased with the concentration of FMD (R = 0.80, Fig. 6a), consistent with the important role of mineral dust, particularly feldspar-bearing particles, in immersion freezing (Kiselev et al., 2017). As part of the compositional analysis, we also examined the behavior of BC. Although BC showed a weak positive correlation with INPs (R = 0.17, Fig. 6b), this relationship became statistically insignificant once FMD was accounted for in a partial correlation analysis (Fig. 6c). This is consistent with laboratory studies showing that BC may nucleate ice mainly under cirrus conditions through deposition freezing (Nichman et al., 2019), while its potential role in immersion freezing warrants further investigation.

~~SNA was quantified as the summed concentration of SO_4^{2-}, NO_3^-, NH_4^+, a commonly used formulation that reflects the overall loading of secondary inorganic aerosol and serves as an indicator of pollution processing (Hu et al., 2017). Specifically, SNA was calculated as:~~

~~with all components expressed as $PM_{2.5}$ mass concentrations.~~ Across all events, INP concentrations decreased with increasing SNA (R = −0.71), whereas this relationship reversed during dust events, where SNA instead showed a positive association with INPs (Fig. 6d). To further investigate this divergence, we examined the ratio of soluble Ca^{2+} to elemental Ca, an indicator of dust dissolution. SNA was positively correlated with this Ca^{2+}/Ca ratio during dust events but showed no relationship in non-dust periods (Fig.7a), indicating that SNA in dust events is linked to the chemical aging of transported mineral particles rather than to local urban pollution. This interpretation is consistent with the low local pollution in Lanzhou and with evidence that SNA on Asian dust is primarily controlled by chemical aging along its transport pathway (Li et al., 2015). Notably, the Ca^{2+}/Ca ratio itself shows little association with INP concentrations (Fig. 7b). This agrees with field evidence showing that increases in water-soluble ions through pollution-induced aging do not necessarily translate into stronger ice-nucleating activity (Chen et al., 2023). Instead, the positive SNA–INP relationship observed during dust events (Fig. 7c) likely reflects their joint increase with dust intrusion intensity: stronger dust episodes elevate both mineral dust loading and SNA levels.

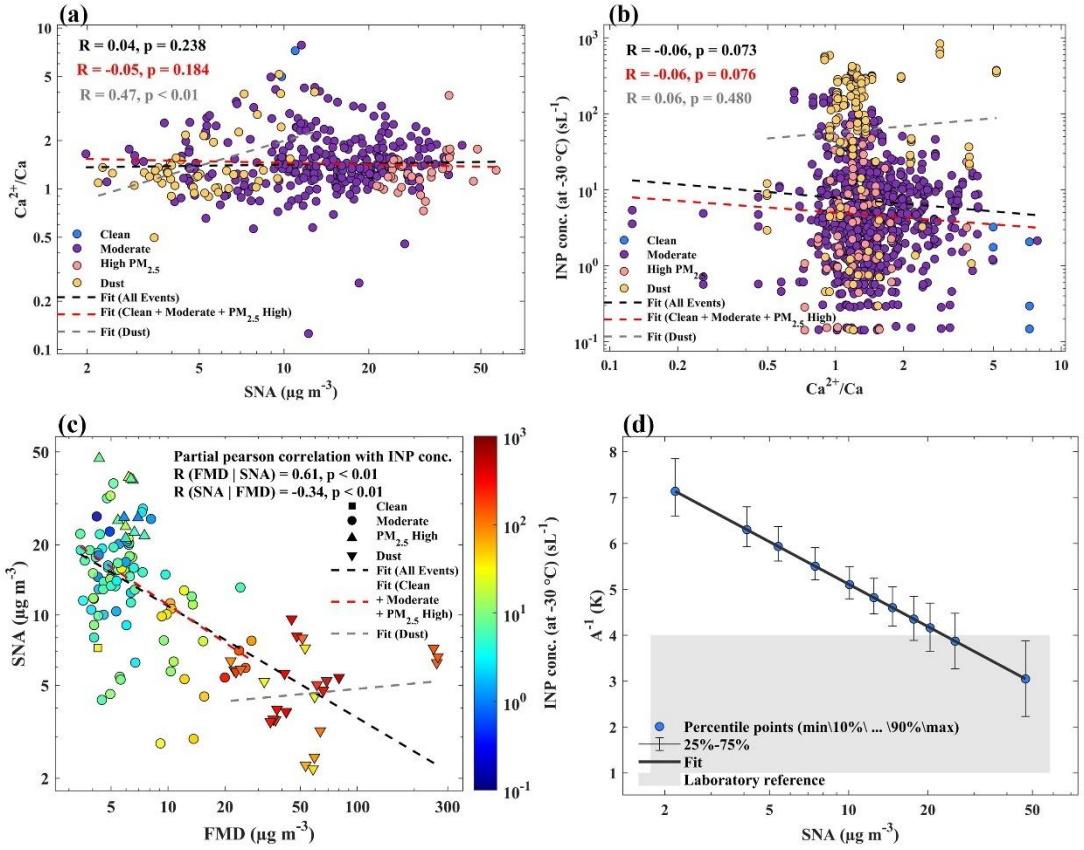

Fig. 7. Associations between -30 °C INP concentrations and SNA. (a) Scatter plots of SNA versus Ca^{2+}/Ca. (b) Scatter plots of Ca^{2+}/Ca versus INP concentrations. *R* denotes the Pearson correlation coefficient and *p* the significance level, calculated in the natural log space. (c) Bivariate plots with FMD and SNA on the axes, where the color scale represents INP concentrations. *R* and *p* denote the partial correlation coefficient and significance level, also calculated in the natural log space. (d) Dependence of the sensitivity metric A^{-1} on SNA concentrations (−25 °C to −35 °C). The shaded area indicates the laboratory reference range reported by Villanueva et al. (2025).

A key issue, however, is that the negative SNA–INP relationship persists even after transported-dust events are removed, and even in partial correlation analyses that control for FMD to account for the temporal mismatch (Fig. 7c). This indicates that, under non-dust-transport conditions, elevated SNA corresponds to an aerosol regime in which efficient mineral-dust INPs are relatively scarce. Consistent with this interpretation, INP concentrations during $PM_{2.5}$ High conditions tend to be lower than those during Moderate conditions, although the difference is not statistically significant (Fig. 3d). This slight decrease may suggest that mineral dust present under polluted conditions has experienced physicochemical modification, which in turn modulates its ice-nucleating efficiency. Secondary inorganic coatings (e.g., $(NH_4)_2SO_4$) can increase the effective contact angles on mineral surfaces, thereby requiring higher supersaturation for activation (Eastwood et al., 2009; Chernoff and Bertram, 2010). H_2SO_4 coatings can even irreversibly suppress the ice-nucleating activity of mineral dust (Sullivan et al., 2010),

indicating that anthropogenic SO_2 and NH_3 emissions can substantially alter the immersion-freezing efficiency of dust particles. At the same time, other studies have reported that the ice-nucleating activity of mineral dust is not necessarily reduced after atmospheric aging, and in some cases remains largely unchanged or even partially enhanced, depending on the chemical composition and extent of surface processing (Kanji et al., 2019; Bertozzi et al., 2021; Chen et al.,2023; Huang et al.,2025). For example, field observations in Beijing reported no systematic difference in mineral-dust-related INP activity between polluted and clean conditions (Chen et al., 2018; Zhang et al., 2022). ~~Consistent with this, Fig. 3d also shows that INP abundances during $PM_{2.5}$ High periods are lower than during moderate pollution conditions.~~ Taken together, these results indicate that, although pollution aerosols are not efficient immersion freezing INPs, they may still influence the observed INP abundance indirectly when pollution loading is high and mineral dust is scarce.

Beyond the correlation analysis~~Considering that temperature variability may also influence the observed correlations between INPs and aerosol components~~, this study further evaluated the sensitivity of INPs to dust under different levels of SNA loading. We use the sensitivity metric A^{-1} from Villanueva et al. (2025), defined as the ratio of dust to temperature sensitivity, with a slight modification here to include SNA (see Appendix Text S3). At the median SNA level (12.47 μg m^{-3}), A^{-1} equals 4.82 K, meaning that increasing dust by e-fold (i.e., based on the natural exponential e) would produce the same INP enhancement as lowering the temperature by approximately 4.82 K (Fig. 7d). As SNA concentrations increase, this A^{-1} declines from about 6.30 K at the 10th percentile of SNA (4.10 μg m^{-3}) to about 3.87 K at the 90th percentile (25.41 μg m^{-3}), corresponding to a reduction of ~39%.

3.54 $n_{1.0}$-based INP parameterizations

INP concentrations decrease systematically with increasing temperature and exhibit pronounced variability across different aerosol regimes. These features indicate the need for a quantitative framework describing the relationships between INP concentrations, thermodynamic conditions, and aerosol properties. Following established temperature-based parameterization approaches (Meyers et al., 1992; Demott et al.,2010), empirical relationships are fitted and evaluated using the present dataset.~~T~~ A temperature-only formulation is first examined, followed by an extension of the framework that incorporates coarse-mode particle concentrations as an additional predictor~~o capture variability across aerosol types, we refined empirical INP parameterizations, progressing from a temperature based model to a two parameter scheme incorporating coarse mode particle concentrations~~ (see Appendix Text S2).

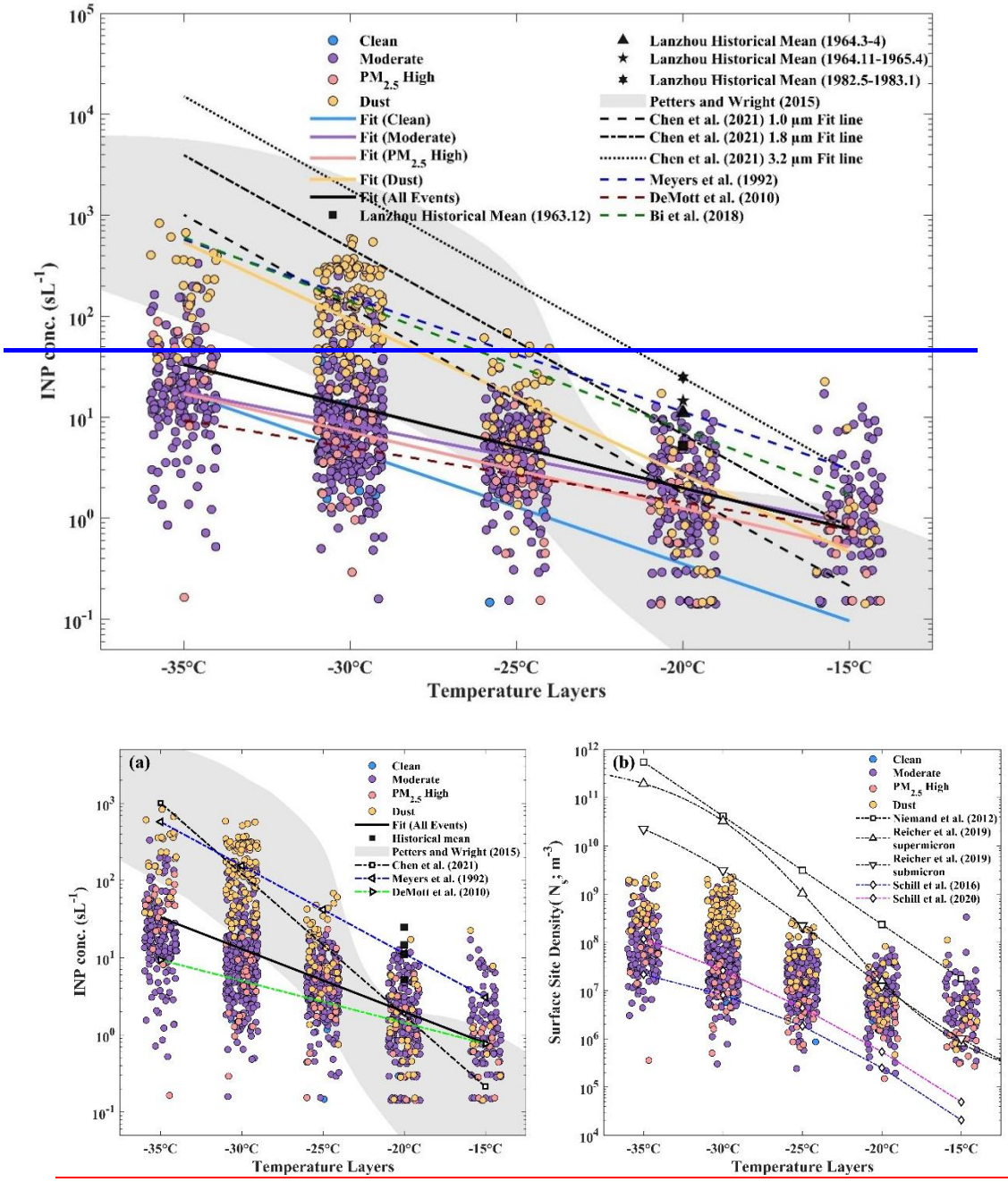

Fig. 8. Construction of single-parameter INPs parameterizations and comparison with existing parameterization schemes. (a) Temperature dependence of INP concentrations. The black solid line shows the overall fit from all events, and representative literature parameterizations are included for comparison. The gray shaded region denotes the range reported by Petters and Wright (2015). The black square indicates the historical mean INP concentration in Lanzhou (Ge et al., 1986).~~Gray shading indicates the global precipitation-derived INP concentrations. Gray dashed lines represent predictions from existing parameterizations. Gray dots indicate historical mean INP~~

~~concentrations in Lanzhou from the 1960s to 1980s (Ge et al., 1986).~~

A temperature-only parameterization was fitted at the five temperature layers (Fig. 8a). The fitted exponential relationship captures the systematic decrease of INP concentrations with increasing temperature and reproduces the overall magnitude of the observations. Substantial dispersion remains at each temperature layer, and the spread increases toward colder temperatures, with INP concentrations spanning about two orders of magnitude at −25 °C and warmer and approaching three orders of magnitude at colder temperatures. This enhanced dispersion is consistent with increasingly distinct INP activities among different aerosol regimes. Dust events occupy the upper range of observed INP concentrations and display steeper temperature dependences than non-dust regimes, consistent with typical mineral dust behavior (Beall et al., 2022). In contrast, Clean, Moderate, and $PM_{2.5}$ High events largely overlap and collectively exhibit lower INP concentrations. Several widely used temperature-based parameterizations are also shown. The shaded envelope representing precipitation-derived INP concentrations reported by Petters and Wright (2015) overlaps with many of the observations, placing the Lanzhou dataset within the typical global range. ~~To capture variability across aerosol types, we refined empirical INP parameterizations, progressing from a temperature-based model to a two-parameter scheme incorporating coarse-mode particle concentrations (see Appendix Text S2). The slopes vary markedly, with dust events exhibiting the steepest increase (Fig. 8), highlighting the strong temperature sensitivity of dust-related INPs, consistent with typical mineral dust behavior (Beall et al., 2022). A comparison of the INPs temperature relationships across aerosol types with existing parameterizations shows that local observations generally fall within established ranges.~~ The fitted curve for dust events aligns with the Beijing dust scheme proposed by Chen et al. (2021) under the 1.0 ~~μm~~μm cutoff, but lies below those based on 1.8 ~~μm~~μm and 3.2 ~~μm~~μm thresholds In contrast, non-dust types closely match the global mean parameterization of DeMott et al. (2010), reflecting background-like nucleation behavior. This apparent consistency based on temperature alone does not necessarily imply common sources or nucleation efficiencies. Historical INPs observations at −30 °C from Lanzhou (1960s–1980s) also fall within the same order of magnitude, though slightly higher than present results, likely due to methodological differences and subsequent improvements in data quality. A complete summary of all fitted parameters is provided in Table S2~~1~~.

Temperature-dependent N_s relationships are also presented in Fig. 8b. During Dust events, the derived N_s values are systematically lower than mineral-dust-based parameterizations (Niemand et al., 2012), typically by about 1–2 orders of magnitude. Such discrepancies are expected, as laboratory-derived schemes are known to represent fresh mineral surfaces and tend to overestimate ambient N_s (Connolly et al., 2009; Ullrich et al., 2017). In comparison, the observed Dust-event N_s values are closer to the lower bound of the size-segregated parameterizations proposed by Reicher et al. (2019), particularly the submicron scheme. For Clean, Moderate, and $PM_{2.5}$ High events, the observed N_s values fall largely within the range predicted by combustion-related parameterizations for vehicle exhaust and biomass-burning aerosols (Schill et al., 2016; 2020), while remaining substantially lower than mineral-dust-based schemes. The pronounced variability in ice-nucleating efficiency across aerosol regimes indicates that temperature-only parameterizations are insufficient. An improved framework should either adopt

aerosol-type-specific parameterizations or incorporate aerosol-related indicators that distinguish between dust-influenced and pollution-influenced conditions.

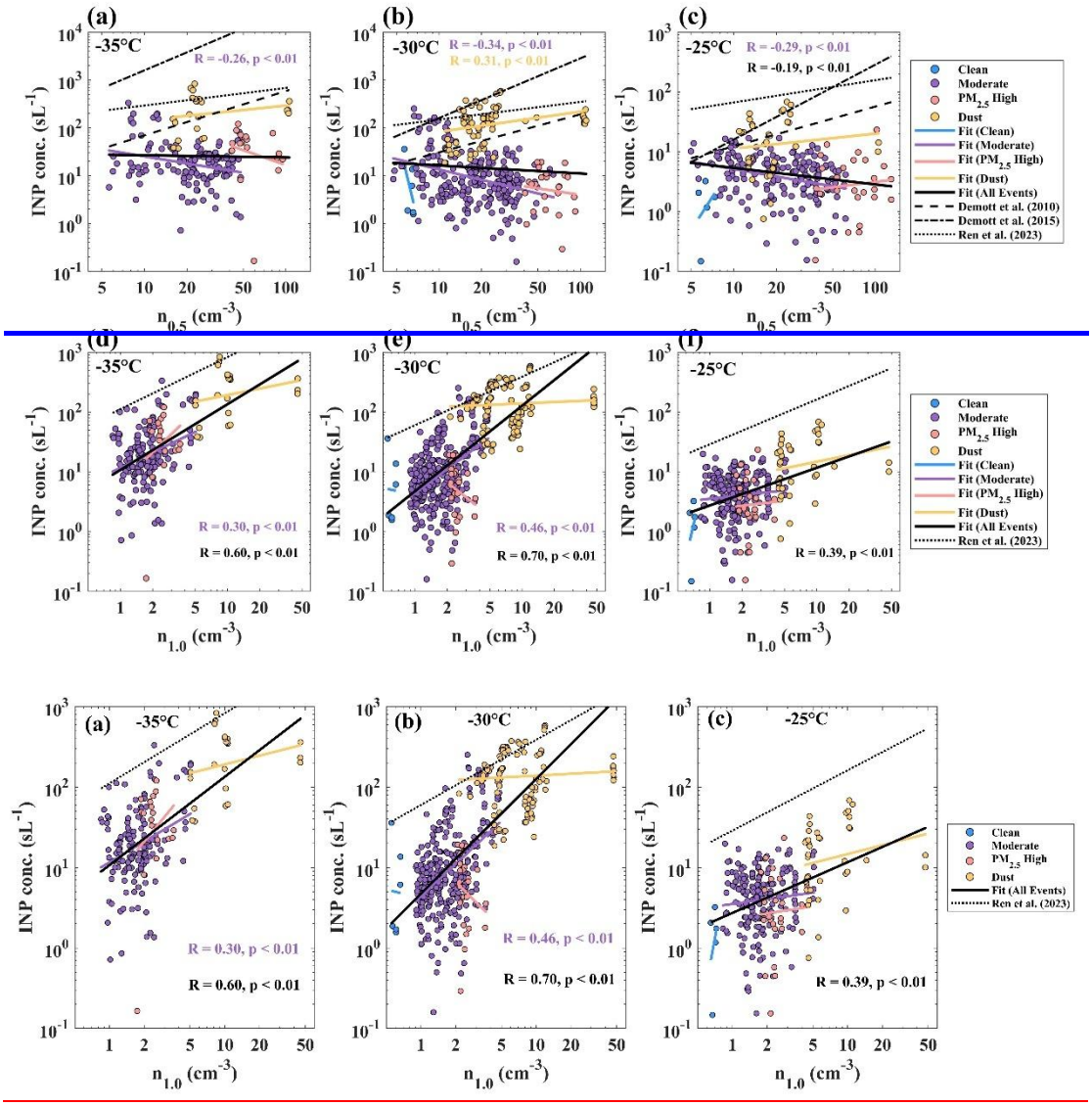

Fig. 9. Relationships between INPs and aerosol number concentrations. (a–c) show the relationships between INP concentrations and n_{0}1.0.5, while (d–f) depict the relationships with n1.0. The black dashed line indicates the prediction from existing parameterization schemes. The *R* and *p* values represent the Pearson correlation coefficient and its significance, and only results with p < 0.01 are shown.

When all aerosol event types are combined (Fig. 9a–f), INP concentrations at colder temperatures (−25 °C to −35 °C) show a significant positive correlation with $n_{1.0}$ (particle number concentration with D = 1.0–2.5 μmμm), which is generally stronger than with $n_{0.5}$ (particle number concentration with D = 0.5–2.5 μmμm, Fig. S12). Because FMD, which represents an

important contributor to active sites, shows a strong positive correlation with $n_{1.0}$ (R = 0.90, Fig. S138) but a negative correlation with $n_{0.5}$ (R = −0.19), using $n_{1.0}$ simply provides a size metric that better matches the dust characteristics in this region. This agrees with earlier urban observations indicating that $n_{0.5}$ is not a reliable predictor of INPs because it reflects background aerosols rather than the larger particles typically responsible for ice nucleation in polluted regions (Chen et al., 2018; Wagh et al., 2021). At warmer temperatures (−15 °C and −20 °C), INP concentrations were near the detection limit, and correlations with $n_{1.0}$ and $n_{0.5}$ were weak (Fig. S149); thus, the parameterizations at these temperatures should be interpreted with caution. Nevertheless, data from all temperatures were retained to ensure full representativeness in this study (see Table S32 for the specific formulae).

We further examined the relationships between INP concentrations and particle number concentrations across different size intervals within each aerosol event type (Fig. S150). Across all five activation temperatures, no particle-size range showed a statistically significant association with INPs in either Clean or $PM_{2.5}$ High events. For Dust events, significant positive correlations emerged only at −30 °C, and only for particles in the 0.25–0.5 ~~μm~~μm and 0.5–1.0 ~~μm~~μm intervals. Accordingly, we did not extend the temperature-based fits with an additional size-dependent predictor within individual event categories.

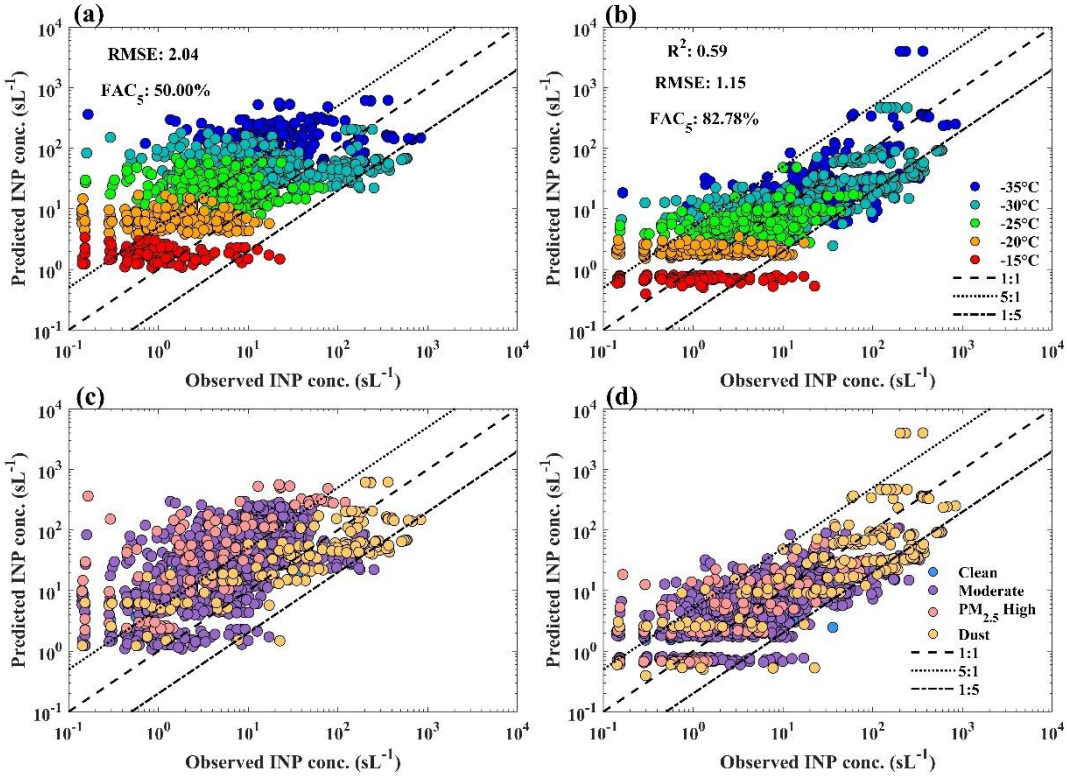

Fig. 10. Comparison between predicted and observed INP concentrations. (a) and (c) show the prediction results of the D10 parameterization scheme using $n_{0.5}$ as input across different temperature conditions, while (b) and (d) present the corresponding predictions from the exponential model developed in this study based on $n_{1.0}$. The black solid line denotes the 1:1 reference line, and the gray dashed lines indicate the ±5-fold error bounds.

To evaluate the performance of the parameterizations, three metrics were applied: RMSE, FAC_5 (fraction of data points falling within the ±5-fold error range), and R^2 (definitions in Appendix Text S4). The global mean parameterization dual-parameter scheme systematically overestimates INP concentrations, yielding an RMSE of 2.04 and an FAC_5 of 50% (Fig. 10). These biases were most evident at colder activation temperatures and during pollution-dominated periods, underscoring the importance of accounting for urban aerosol event types~~conditions~~ when applying global INP parameterizations. By comparison, the locally derived $n_{1.0}$-based model achieves markedly improved skill (R^2 = 0.59, RMSE = 1.15, FAC_5 = 82.8%), providing higher predictive accuracy and greater consistency across both temperature regimes and aerosol event types. Nevertheless, certain limitations remain. The vertical alignment of observed INP concentrations at approximately 0.13 sL^{-1} reflects the instrumental detection limit of the CFDC measurements. At −15 °C, the current parameterization does not capture aerosol-related variability and effectively yields a single representative value. Despite these limitations, the overall~~Importantly, this~~ improvement mainly reflects a regional optimization that better suits the urban environment, suggesting that parameterizations may benefit from incorporating region-specific aerosol characteristics when applied to complex environments. In addition, future coordinated online CFDC and offline droplet-freezing measurements may help better constrain low-level INP concentrations.

4. Conclusion

B~~Ice-nucleating particles (INPs) play a crucial role in cloud microphysical processes and precipitation formation, as they serve as the critical agents for initiating ice formation in clouds (Hoose and Möhler, 2012; Hawker et al., 2021). The temporal variation of INPs in urban atmospheres and their relationship with aerosol properties are gaining increasing attention in the context of climate change and urbanization (Tobo et al., 2020; Hu et al., 2023). However, systematic studies based on high-temporal resolution observations are notably scarce in urban inland areas, particularly in arid and semi-arid regions (Jiang et al., 2016). Therefore, b~~ased on the first winter-spring, high-time-resolution online INP measurements in Lanzhou, this study investigated the temporal variability and controlling factors of INPs in an urban inland environment. ~~The specific conclusions of this article are as follows.~~

Springtime dust storms elevate INP concentrations at −30 °C by a factor of ~15, making episodic dust plumes the primary driver of urban INP bursts. In contrast, $PM_{2.5}$-rich pollution episodes only contribute significant ice-nucleating ability below −35 °C~~0.0~~, revealing a clear “dust-warm vs pollutant-cold” temperature threshold that can be used to flag dominant INP sources in operational forecasts. Normalized activation fractions and surface site densities confirm that the elevated INP concentrations during dust events are attributable to intrinsically higher ice-nucleating efficiency of mineral dust, rather than merely increased particle abundance. Backward trajectory and land-cover analyses further show that elevated INPs are linked to long-range transport from arid source regions, while $PM_{2.5}$ High events are mainly associated with near-regional air masses.

Urban-inland INP bursts are driven by episodic dust plumes, not persistent $PM_{2.5}$~~, as revealed by the first winter–spring online INP record in Lanzhou~~. Fine mineral dust (FMD) provides a robust indicator of dust-related INP contributions, whereas

secondary inorganic aerosol accumulated during pollution events correlates negatively with INP activity. While our −30 °C observations show a strong negative correlation between SNA mass and INP number (R = −0.71), this consistency is circumstantial. Ambient RH, coating thickness, and dust mineralogy were not constrained, and the relationship emerged only under conditions where pollution levels were high and dust influence was relatively weak. Therefore, the degree to which coatings suppress INPs in the real atmosphere remains an open question requiring targeted follow-up studies.

Although a temperature-only scheme reproduces the overall thermal trend of INPs, the pronounced dispersion, particularly at colder temperatures, and the clear separation between dust and non-dust regimes indicate that temperature alone cannot account for urban INP variability. temperature-dependent N_s comparisons further reveal strong aerosol-type dependence of ice-nucleating efficiency, highlighting the limitation of temperature-only parameterizations. Because FMD is closely associated with $n_{1.0}$ ($R = 0.90$), using $n_{1.0}$ as the size indicator provides a more regionally representative basis for INP estimation in this urban environment. Building on this, the two-parameter framework demonstrates stable performance across different aerosol event types~~conditions~~ and temperatures, achieving RMSE = 1.15, FAC_5 = 82.78%, and R^2 = 0.59. Overall, the scheme benefits from the fact that particle size can partially reflect aerosol types and, in turn, their associated ice-nucleating activity, providing a practical approach for estimating regional INP concentrations. ~~Given the local conditions, current parameterizations may face limitations, warranting multi-site evaluation of their transferability.~~

This study could provide region-specific constraints on aerosol–ice-cloud interactions in arid North-West China and offer observational insights that can inform parameterizations for other dryland cities where urban air interacts with transported dust.~~a transferable parameterization for similar dryland cities worldwide.~~ We demonstrate that particle size alone can distinguish dust-dominated from pollution-dominated INP sources in a dryland city. However, extending the scheme to humid subtropical or marine-coastal regions will require multi-site validation and inclusion of additional parameters (e.g., mineralogical composition, organic-mass fraction). Such coordinated efforts will enable more accurate INP representation in regional and global models that presently overlook non-marine, non-pure-desert ice-nucleating sources, ultimately improving our ability to simulate cloud formation and climate feedbacks across diverse atmospheric environments.

Data availability

Datasets used to generate the figures in this study are available on Zenodo (https://doi.org/10.5281/zenodo.17775917). Other measurement datasets used in this study can be obtained from the corresponding author on reasonable request. Meteorological fields used for the HYSPLIT simulations are publicly available from the NOAA Air Resources Laboratory (https://www.ready.noaa.gov).

Author Contribution.

C.C. designed the study, performed the field INP measurements, and conducted the analysis of the related aerosol observational

datasets. Ya.W. and J.L. supervised the research and provided guidance on methodology and interpretation. L.F. and T.C. assisted with aerosol instrumentation maintenance and data preprocessing. Z.J. contributed to the ion chromatography and heavy-metal data acquisition. J.W. and Yu.W. provided model support and contributed to the discussion of the parameterization framework. J.H. offered conceptual guidance on regional aerosol–cloud interactions and contributed to interpretation of the results. C.C. wrote the manuscript with input from all authors. All authors reviewed and approved the final manuscript.

Competing interests.

The authors declare that they have no conflict of interest.

Financial support.

This work is supported by the Innovative Research Group Project of the National Natural Science Foundation of China (42421001), the Science and Technology Project of Gansu Province (Outstanding Youth Fund, 24JRRA386), the National Natural Science Foundation of China (42575083), and the NSFC Regional Innovation and Development Joint Fund (U24A20604).

Acknowledgments.

We gratefully acknowledge the support of the Lanzhou University Supercomputing Center. We also acknowledge the NOAA Air Resources Laboratory for providing the HYSPLIT transport and dispersion model and the associated meteorological data used in this study.

Reference

Baron, P. A. and Willeke, K. (Eds.): Aerosol Measurement: Principles, Techniques, and Applications, 3rd ed., Wiley, ISBN 9780470387412, 2011.

Barry, K. R., Hill, T. C. J., Levin, E. J. T., Twohy, C. H., Moore, K. A., Weller, Z. D., Toohey, D. W., Reeves, M., Campos, T., Geiss, R., Schill, G. P., Fischer, E. V., Kreidenweis, S. M., and DeMott, P. J.: Observations of ice nucleating particles in the free troposphere from western US wildfires, J. Geophys. Res. Atmos., 126, e2020JD033752, doi:10.1029/2020JD033752, 2021.

Beall, C. M., Hill, T. C. J., DeMott, P. J., Köneman, T., Pikridas, M., Drewnick, F., Harder, H., Pöhlker, C., Lelieveld, J., Weber, B., Iakovides, M., Prokeš, R., Sciare, J., Andreae, M. O., Stokes, M. D., and Prather, K. A.: Ice-nucleating particles near two major dust source regions, Atmos. Chem. Phys., 22, 12607–12627, doi:10.5194/acp-22-12607-2022, 2022.

Bertozzi, B., Wagner, R., Song, J., Höhler, K., Pfeifer, J., Saathoff, H., Leisner, T., and Möhler, O.: Ice nucleation ability of ammonium sulfate aerosol particles internally mixed with secondary organics, Atmos. Chem. Phys., 21, 10779–10798, doi:10.5194/acp-21-10779-2021, 2021.

~~Bi, K., Ma, X., Chen, Y., Fu, S., and Xue, H.: The observation of ice-nucleating particles active at temperatures above −15 °C and its implication on ice formation in clouds, J. Meteorol. Res., 32, 734–743, doi:10.1007/s13351-018-7181-z, 2018.~~

Bi, K., McMeeking, G. R., Ding, D. P., Levin, E. J. T., DeMott, P. J., Zhao, D. L., Wang, F., Liu, Q., Tian, P., Ma, X. C., Chen, Y. B., Huang, M. Y., Zhang, H. L., Gordon, T. D., and Chen, P.: Measurements of ice nucleating particles in Beijing, China, J. Geophys. Res. Atmos., 124, 8065–8075, doi:10.1029/2019JD030609, 2019.

Burrows, S. M., McCluskey, C. S., Cornwell, G., Steinke, I., Zhang, K., Zhao, B., Zawadowicz, M., Raman, A., Kulkarni, G., China, S., Zelenyuk, A., and DeMott, P. J.: Ice-nucleating particles that impact clouds and climate: observational and modeling research needs, Rev. Geophys., 60, e2021RG000745, doi:10.1029/2021RG000745, 2022.

Chatziparaschos, M., Daskalakis, N., Myriokefalitakis, S., Kalivitis, N., Nenes, A., Gonçalves Ageitos, M., Costa-Surós, M., Pérez García-Pando, C., Zanoli, M., Vrekoussis, M., and Kanakidou, M.: Role of K-feldspar and quartz in global ice nucleation by mineral dust in mixed-phase clouds, Atmos. Chem. Phys., 23, 1785–1801, doi:10.5194/acp-23-1785-2023, 2023.

Chen, J., Wu, Z., Augustin-Bauditz, S., Grawe, S., Hartmann, M., Pei, X., Liu, Z., Ji, D., and Wex, H.: Ice-nucleating particle concentrations unaffected by urban air pollution in Beijing, China, Atmos. Chem. Phys., 18, 3523–3539, doi:10.5194/acp-18-3523-2018, 2018.

Chen, J., Wu, Z., Chen, J., Reicher, N., Fang, X., Rudich, Y., and Hu, M.: Size-resolved atmospheric ice-nucleating particles during East Asian dust events, Atmos. Chem. Phys., 21, 3491–3506, doi:10.5194/acp-21-3491-2021, 2021.

Chen, J., Wu, Z., Meng, X., Zhang, C., Chen, J., Qiu, Y., Chen, L., Fang, X., Wang, Y., Zhang, Y., Chen, S., Gao, J., Li, W., and Hu, M.: Observational evidence for the non-suppression effect of atmospheric chemical modification on the ice nucleation activity of East Asian dust, Sci. Total Environ., 861, 160708, doi:10.1016/j.scitotenv.2022.160708, 2023.

Chen, J., Xu, J., Wu, Z., Meng, X., Yu, Y., Ginoux, P., DeMott, P. J., Xu, R., Zhai, L., Yan, Y., Zhao, C., Li, S.-M., Zhu, T., and Hu, M.: Decreased dust particles amplify the cloud cooling effect by regulating cloud ice formation over the Tibetan Plateau, Sci. Adv., 10, eado0885, doi:10.1126/sciadv.ado0885, 2024a.

Chen, J., Wu, Z., Gong, X., Qiu, Y., Chen, S., Zeng, L., and Hu, M.: Anthropogenic dust as a significant source of ice-nucleating particles in the urban environment, Earth's Future, 12, e2023EF003738, doi:10.1029/2023EF003738, 2024b.

Chen, J., Jakob, F. M. O., Voliotis, A., Wu, H., Syafira, S. A., Oghama, O., Shardt, N., Fauré, N., Kong, X., McFiggans, G., and Kanji, Z. A.: Ice nucleation abilities and chemical characteristics of laboratory-generated and aged biomass burning aerosols, Environ. Sci. Technol., 59, 2575–2586, doi:10.1021/acs.est.4c04941, 2025.

Chen, S., Zhang, X., Lin, J., Huang, J., Zhao, D., Yuan, T., Huang, K., Luo, Y., Jia, Z., Zang, Z., Qiu, Y., and Xie, L.: Fugitive road dust PM2.5 emissions and their potential health impacts, Environ. Sci. Technol., 53, 8455–8465, doi:10.1021/acs.est.9b00666, 2019.

Cheng, B., Ma, Y., Li, H., Feng, F., Zhang, Y., and Qin, P.: Water-soluble ions and source apportionment of PM2.5 depending on synoptic weather patterns in an urban environment in spring dust season, Sci. Rep., 12, 21953, doi:10.1038/s41598-022-26615-y, 2022.

Chernoff, D. I. and Bertram, A. K.: Effects of sulfate coatings on the ice nucleation properties of a biological ice nucleus and several types of minerals, J. Geophys. Res. Atmos., 115, D20207, doi:10.1029/2010JD014254, 2010.

Connolly, P. J., Möhler, O., Field, P. R., Saathoff, H., Burgess, R., Choularton, T., and Gallagher, M.: Studies of heterogeneous freezing by three different desert dust samples, Atmos. Chem. Phys., 9, 2805–2824, https://doi.org/10.5194/acp-9-2805-2009, 2009.

Creamean, J. M., Barry, K., Hill, T. C. J., Hume, C., DeMott, P. J., Shupe, M. D., Dahlke, S., Willmes, S., Schmale, J., Beck, I., Hoppe, C. J. M., Fong, A., Chamberlain, E., Bowman, J., Scharien, R., and Persson, O.: Annual cycle observations of aerosols capable of ice formation in central Arctic clouds, Nat. Commun., 13, 3537, doi:10.1038/s41467-022-31182-x, 2022.

DeMott, P. J., Prenni, A. J., Liu, X., Kreidenweis, S. M., Petters, M. D., Twohy, C. H., Richardson, M. S., Eidhammer, T., and Rogers, D. C.: Predicting global atmospheric ice nuclei distributions and their impacts on climate, Proc. Natl. Acad. Sci. U.S.A., 107, 11217–11222, doi:10.1073/pnas.0910818107, 2010.

DeMott, P. J., Prenni, A. J., McMeeking, G. R., Sullivan, R. C., Petters, M. D., Tobo, Y., Niemand, M., Möhler, O., Snider, J. R., Wang, Z., and Kreidenweis, S. M.: Integrating laboratory and field data to quantify the immersion freezing ice nucleation activity of mineral dust particles, Atmos. Chem. Phys., 15, 393–409, doi:10.5194/acp-15-393-2015, 2015.

DeMott, P. J., Hill, T. C. J., Petters, M. D., Bertram, A. K., Tobo, Y., Mason, R. H., Suski, K. J., McCluskey, C. S., Levin, E. J. T., Schill, G. P., Boose, Y., Rauker, A. M., Miller, A. J., Zaragoza, J., Rocci, K., Rothfuss, N. E., Taylor, H. P., Hader, J. D., Chou, C., and Kreidenweis, S. M.: Comparative measurements of ambient atmospheric concentrations of ice nucleating particles using multiple immersion freezing methods and a continuous flow diffusion chamber, Atmos. Chem. Phys., 17, 11227–11245, doi:10.5194/acp-17-11227-2017, 2017.

DeMott, P. J., Mirrielees, J. A., Petters, S. S., Cziczo, D. J., Petters, M. D., Bingemer, H. G., Hill, T. C. J., Froyd, K., Garimella, S., Hallar, A. G., Levin, E. J. T., McCubbin, I. B., Perring, A. E., Rapp, C. N., Schiebel, T., Schrod, J., Suski, K. J., Weber, D., Wolf, M. J., and Brooks, S. D.: Field intercomparison of ice nucleation measurements: The fifth international workshop on ice nucleation phase 3 (FIN-03), Atmos. Meas. Tech., 18, 639–672, doi:10.5194/amt-18-639-2025, 2025.

Du, T., Wang, M., Guan, X., Zhang, M., Zeng, H., Chang, Y., Zhang, L., Tian, P., Shi, J., and Tang, C.: Characteristics and formation mechanisms of winter particulate pollution in Lanzhou, Northwest China, J. Geophys. Res. Atmos., 125, e2020JD033369, doi:10.1029/2020JD033369, 2020.

Eastwood, M. L., Cremel, S., Wheeler, M., Murray, B. J., Girard, E., and Bertram, A. K.: Effects of sulfuric acid and ammonium sulfate coatings on the ice nucleation properties of kaolinite particles, Geophys. Res. Lett., 36, L02503, doi:10.1029/2008GL035997, 2009.

Field, P. R. and Heymsfield, A. J.: Importance of snow to global precipitation, Geophys. Res. Lett., 42, 9512–9520, doi:10.1002/2015GL065497, 2015

French, J. R., Friedrich, K., Tessendorf, S. A., Rauber, R. M., Geerts, B., Rasmussen, R. M., Xue, L., Kunkel, M. L., and Blestrud, D. R.: Precipitation formation from orographic cloud seeding, Proc. Natl. Acad. Sci. U.S.A., 115, 1168–1173, doi:10.1073/pnas.1716995115, 2018.

Ge, Z. and Zhou, C.: The observations of atmospheric ice nuclei in Lanzhou, Plateau Meteorol., 5, 167–171, available at: http://www.gyqx.ac.cn/CN/Y1986/V5/I2/167, 1986.

Gjelsvik, A. B., David, R. O., Carlsen, T., Hellmuth, F., Hofer, S., McGraw, Z., Sodemann, H., Storelvmo, T.: Using a region-specific ice-nucleating particle parameterization improves the representation of Arctic clouds in a global climate model, Atmos. Chem. Phys., 25, 1617–1637, doi:10.5194/acp-25-1617-2025, 2025.

Hawker, R. E., Miltenberger, A. K., Wilkinson, J. M., Hill, A. A., Shipway, B. J., Cui, Z., Cotton, R. J., Carslaw, K. S., Field, P. R., and Murray, B. J.: The temperature dependence of ice-nucleating particle concentrations affects the radiative properties of tropical convective cloud systems, Atmos. Chem. Phys., 21, 5439–5461, doi:10.5194/acp-21-5439-2021, 2021.

Herbert, R. J., Sanchez-Marroquin, A., Grosvenor, D. P., Pringle, K. J., Arnold, S. R., Murray, B. J., and Carslaw, K. S.: Gaps in our understanding of ice-nucleating particle sources exposed by global simulation of the UK Earth System Model, Atmos. Chem. Phys., 25, 291–325, doi:10.5194/acp-25-291-2025, 2025.

Hinds, W. C.: Aerosol Technology: Properties, Behavior, and Measurement of Airborne Particles, 2nd ed., Wiley-Interscience, ISBN 9781119494041, 1999.

Hiranuma, N., Augustin-Bauditz, S., Bingemer, H., Budke, C., Curtius, J., Danielczok, A., Diehl, K., Dreischmeier, K., Ebert, M., Frank, F., Hoffmann, N., Kandler, K., Kiselev, A., Koop, T., Leisner, T., Möhler, O., Nillius, B., Peckhaus, A., Rose, D., Weinbruch, S., Wex, H., Yamashita, K., and Möhler, O.: A comprehensive laboratory study on the immersion freezing behavior of illite NX particles: A comparison of 17 ice nucleation measurement techniques, Atmos. Chem. Phys., 15, 2489–2518, doi:10.5194/acp-15-2489-2015, 2015.

Hofer, J., Seifert, P., Liley, J. B., Radenz, M., Uchino, O., Morino, I., Sakai, T., Nagai, T., and Ansmann, A.: Aerosol-related effects on the occurrence of heterogeneous ice formation over Lauder, New Zealand/Aotearoa, Atmos. Chem. Phys., 24, 1265–1280, https://doi.org/10.5194/acp-24-1265-2024, 2024.

Hoose, C. and Möhler, O.: Heterogeneous ice nucleation on atmospheric aerosols: A review of results from laboratory experiments, Atmos. Chem. Phys., 12, 9817–9854, doi:10.5194/acp-12-9817-2012, 2012.

Hu, W., Hu, M., Hu, W.-W., Zheng, J., Chen, C., Wu, Y., and Guo, S.: Seasonal variations in high time-resolved chemical compositions, sources, and evolution of atmospheric submicron aerosols in the megacity Beijing, Atmos. Chem. Phys., 17, 9979–10000, https://doi.org/10.5194/acp-17-9979-2017, 2017.

Hu, Y., Tian, P., Huang, M., Bi, K., Schneider, J., Umo, N. S., Ullmerich, N., Höhler, K., Jing, X., Xue, H., Ding, D., Liu, Y., Leisner, T., and Möhler, O.: Characteristics of ice-nucleating particles in Beijing during spring: a comparison study of measurements between the suburban and a nearby mountain area, Atmos. Environ., 293, 119451, doi:10.1016/j.atmosenv.2022.119451, 2023.

Huang, Z., Hu, W., Chen, J., Zhu, J., Wu, Z., Zhang, Y., and Fu, P.: Atmospheric aging effects on aerosol ice nucleation, Earth-Sci. Rev., 269, 105176, doi:10.1016/j.earscirev.2025.105176, 2025.

Jiang, H., Yin, Y., Wang, X., Gao, R., Yuan, L., Chen, K., and Shan, Y.: The measurement and parameterization of ice nucleating particles in different backgrounds of China, Atmos. Res., 181, 72–80, doi:10.1016/j.atmosres.2016.06.013, 2016.

Kanji, Z. A., DeMott, P. J., Möhler, O., and Abbatt, J. P. D.: Results from the University of Toronto continuous flow diffusion chamber at ICIS 2007: Instrument intercomparison and ice onsets for different aerosol types, Atmos. Chem. Phys., 11, 31–41, https://doi.org/10.5194/acp-11-31-2011, 2011.

Kanji, Z. A., Ladino, L. A., Wex, H., Boose, Y., Burkert-Kohn, M., Cziczo, D. J., and Krämer, M.: Overview of ice nucleating particles, Meteorol. Monogr., 58, 1.1–1.33, doi:10.1175/AMSMONOGRAPHS-D-16-0006.1, 2017.

Kanji, Z. A., Sullivan, R. C., Niemand, M., DeMott, P. J., Prenni, A. J., Chou, C., Saathoff, H., and Möhler, O.: Heterogeneous ice nucleation properties of natural desert dust particles coated with a surrogate of secondary organic aerosol, Atmos. Chem. Phys., 19, 5091–5110, https://doi.org/10.5194/acp-19-5091-2019, 2019.

Kanji, Z. A., Welti, A., Corbin, J. C., and Mensah, A. A.: Black carbon particles do not matter for immersion mode ice nucleation, Geophys. Res. Lett., 47, e2019GL086764, doi:10.1029/2019GL086764, 2020.

Kärcher, B.: A parameterization of cirrus cloud formation: Revisiting competing ice nucleation, J. Geophys. Res. Atmos., 127, e2022JD036907, doi:10.1029/2022JD036907, 2022.

Kawai, K., Matsui, H., and Tobo, Y.: High potential of Asian dust to act as ice nucleating particles in mixed-phase clouds simulated with a global aerosol-climate model, J. Geophys. Res. Atmos., 126, e2020JD034263, doi:10.1029/2020JD034263, 2021.

Kiselev, A., Bachmann, F., Pedevilla, P., Cox, S. J., Michaelides, A., Gerthsen, D., and Leisner, T.: Active sites in heterogeneous ice nucleation—the example of K-rich feldspars, Science, 355, 367–371, doi:10.1126/science.aai8034, 2017.

Lacher, L., Adams, M. P., Barry, K., Bertozzi, B., Bingemer, H., Boffo, C., Bras, Y., Büttner, N., Castarede, D., Cziczo, D. J., DeMott, P. J., Fösig, R., Goodell, M., Höhler, K., Hill, T. C. J., Jentzsch, C., Ladino, L. A., Levin, E. J. T., Mertes, S., and Freney, E.: The puy de dôme ICe nucleation intercomparison campaign (PICNIC): Comparison between online and offline methods in ambient air, Atmos. Chem. Phys., 24, 2651–2678, doi:10.5194/acp-24-2651-2024, 2024.

Lei, H. and Wang, J. X. L.: Observed characteristics of dust storm events over the western United States using meteorological, satellite, and air quality measurements, Atmos. Chem. Phys., 14, 7847–7857, https://doi.org/10.5194/acp-14-7847-2014, 2014.

Levin, E. J. T., McMeeking, G. R., DeMott, P. J., McCluskey, C. S., Stockwell, C. E., Yokelson, R. J., and Kreidenweis, S. M.: A new method to determine the number concentrations of refractory black carbon ice nucleating particles, Aerosol Sci. Technol., 48, 1264–1275, https://doi.org/10.1080/02786826.2014.977843, 2014.

Li, J., Zhang, N., Tian, P., Zhang, M., Shi, J., Chang, Y., Zhang, L., Liu, Z., and Wang, Y.: Significant roles of aged dust aerosols on rapid nitrate formation under dry conditions in a semi-arid city, Environ. Pollut., 336, 122395, doi:10.1016/j.envpol.2023.122395, 2023.

Li, W., Zhou, Y., Zhang, W., Liu, D., Hu, T., Wu, F., Geng, H., and Zhang, D.: A review of water-soluble ions in natural dust particles over East Asia: abundance, spatial distributions, and implications, ACS ES&T Air, 2, 1379–1393, doi:10.1021/acsestair.5c00014, 2025.

Liu, X., Turner, J. R., Hand, J. L., Schichtel, B. A., and Martin, R. V.: A global-scale mineral dust equation, J. Geophys. Res.-Atmos., 127, e2022JD036937, doi:10.1029/2022JD036937, 2022.

Malm, W. C., Sisler, J. F., Huffman, D., Eldred, R. A., and Cahill, T. A.: Spatial and seasonal trends in particle concentration and optical extinction in the United States, J. Geophys. Res., 99, 1347–1370, doi:10.1029/93JD02916, 1994.

McCluskey, C. S., DeMott, P. J., Ma, P.-L., and Burrows, S. M.: Numerical representations of marine ice-nucleating particles in remote marine environments evaluated against observations, Geophys. Res. Lett., 46, 7838–7847, doi:10.1029/2018GL081861, 2019.

McCluskey, C. S., Gettelman, A., Bardeen, C. G., DeMott, P. J., Moore, K. A., Kreidenweis, S. M., Hill, T. C. J., Barry, K. R., Twohy, C. H., Toohey, D. W., Rainwater, B., Jensen, J. B., Reeves, J. M., Alexander, S. P., and McFarquhar, G. M.: Simulating Southern Ocean aerosol and ice nucleating particles in the Community Earth System Model Version 2, J. Geophys. Res. Atmos., 128, e2022JD036955, doi:10.1029/2022JD036955, 2023.

Meyers, M. P., DeMott, P. J., and Cotton, W. R.: New primary ice nucleation parameterizations in an explicit cloud model, J. Appl. Meteorol., 31, 708–721, doi:10.1175/1520-0450(1992)031<0708:NPINPI>2.0.CO;2, 1992.

Moore, K. A., Hill, T. C. J., McCluskey, C. S., Twohy, C. H., Rainwater, B., Toohey, D. W., et al.: Characterizing ice nucleating particles over the Southern Ocean using simultaneous aircraft and ship observations, J. Geophys. Res. Atmos., 129, e2023JD039543, doi:10.1029/2023JD039543, 2024.

Morrison, H., Van Lier-Walqui, M., Fridlind, A. M., Grabowski, W. W., Harrington, J. Y., Hoose, C., Korolev, A., Kumjian, M. R., Milbrandt, J. A., Pawlowska, H., Posselt, D. J., Prat, O. P., Reimel, K. J., Shima, S., Van Diedenhoven, B., and Xue, L.: Confronting the challenge of modeling cloud and precipitation microphysics, J. Adv. Model. Earth Syst., 12, e2019MS001689, doi:10.1029/2019MS001689, 2020.

Murray, J., O'Sullivan, D., Atkinson, J. D., and Webb, M. E.: Ice nucleation by particles immersed in supercooled cloud droplets, Chem. Soc. Rev., 41, 6519–6539, doi:10.1039/c2cs35200a, 2012.

Nichman, L., Wolf, M., Davidovits, P., Onasch, T. B., Zhang, Y., Worsnop, D. R., Bhandari, J., Mazzoleni, C., and Cziczo, D. J.: Laboratory study of the heterogeneous ice nucleation on black-carbon-containing aerosol, Atmos. Chem. Phys., 19, 12175–12194, doi:10.5194/acp-19-12175-2019, 2019.

Niemand, M., Möhler, O., Vogel, B., Vogel, H., Hoose, C., Connolly, P., Klein, H., Bingemer, H., DeMott, P., Skrotzki, J., and Leisner, T.: A Particle-Surface-Area-Based Parameterization of Immersion Freezing on Desert Dust Particles, J. Atmos. Sci., 69, 3077–3092, https://doi.org/10.1175/JAS-D-11-0249.1, 2012.

Pan, B., Liu, D., Tian, P., Zhao, D., Du, Y., Li, S., Hu, K., Hu, D., Sun, B., Yu, C., Chen, Y., Li, W., Huang, M., Xu, H., and You, S.: Increased freezing temperature of clouds over China due to anthropogenic pollution, Geophys. Res. Lett., 51, e2024GL109086, doi:10.1029/2024GL109086, 2024.

Pereira Freitas, G., Adachi, K., Conen, F., Heslin-Rees, D., Krejci, R., Tobo, Y., Yttri, K. E., and Zieger, P.: Regionally sourced bioaerosols drive high-temperature ice nucleating particles in the Arctic, Nat. Commun., 14, 5997, doi:10.1038/s41467-023-41696-7, 2023.

Petters, M. D. and Wright, T. P.: Revisiting ice nucleation from precipitation samples, Geophys. Res. Lett., 42, 8758–8766, doi:10.1002/2015GL065733, 2015.

Phillips, V. T. J., DeMott, P. J., and Andronache, C.: An empirical parameterization of heterogeneous ice nucleation for multiple chemical species of aerosol, J. Atmos. Sci., 65, 2757–2783, doi:10.1175/2007JAS2546.1, 2008.

Pruppacher, H. R., Klett, J. D., and Wang, P. K.: Microphysics of Clouds and Precipitation, Aerosol Sci. Technol., 28, 381–382, doi:10.1080/02786829808965531, 1998.

Ren, Y. Z., Bi, K., Fu, S. Z., Tian, P., Huang, M. Y., Zhu, R. H., and Xue, H. W.: The relationship of aerosol properties and ice-nucleating particle concentrations in Beijing, J. Geophys. Res. Atmos., 128, e2022JD037383, doi:10.1029/2022JD037383, 2023.

Reicher, N., Budke, C., Eickhoff, L., Raveh-Rubin, S., KaplanAshiri, I., Koop, T., and Rudich, Y.: Size-dependent ice nucleation by airborne particles during dust events in the eastern Mediterranean, Atmos. Chem. Phys., 19, 11143–11158, https://doi.org/10.5194/acp-19-11143-2019, 2019.

Richardson, M. S., DeMott, P. J., Kreidenweis, S. M., Petters, M. D., and Carrico, C. M.: Observations of ice nucleation by ambient aerosol in the homogeneous freezing regime, Geophys. Res. Lett., 37, L04804, doi:10.1029/2009GL041912, 2010.

Rivera Rivera, N. I., Gill, T. E., Gebhart, K. A., Hand, J. L., Bleiweiss, M. P., and Fitzgerald, R. M.: Wind modeling of Chihuahuan Desert dust outbreaks, Atmos. Environ., 43, 347–354, doi:10.1016/j.atmosenv.2008.09.069, 2009.

Rogers, D. C., DeMott, P. J., Kreidenweis, S. M., and Chen, Y.: A continuous-flow diffusion chamber for airborne measurements of ice nuclei, J. Atmos. Ocean. Technol., 18, 725–741, doi:10.1175/1520-0426(2001)018<0725:ACFDCF>2.0.CO;2, 2001.

Schill, G. P., Jathar, S. H., Kodros, J. K., Levin, E. J. T., Galang, A. M., Friedman, B., Link, M. F., Farmer, D. K., Pierce, J. R., Kreidenweis, S. M., and DeMott, P. J.: Icenucleating particle emissions from photochemically aged diesel and biodiesel exhaust, Geophys. Res. Lett., 43, 5524–5531, doi:10.1002/2016GL069529, 2016.

Schill, G. P., DeMott, P. J., Emerson, E. W., Rauker, A. M. C., Kodros, J. K., Suski, K. J., Hill, T. C. J., Levin, E. J. T., Pierce, J. R., Farmer, D. K., and Kreidenweis, S. M.: The contribution of black carbon to global ice nucleating particle concentrations relevant to mixed-phase clouds, P. Natl. Acad. Sci. USA, 117, 22705–22711, doi:10.1073/pnas.2001674117, 2020.

Sullivan, R. C., Petters, M. D., DeMott, P. J., Kreidenweis, S. M., Wex, H., Niedermeier, D., Hartmann, S., Clauss, T., Stratmann, F., Reitz, P., Schneider, J., and Sierau, B.: Irreversible loss of ice nucleation active sites in mineral dust particles caused by sulphuric acid condensation, Atmos. Chem. Phys., 10, 11471–11487, doi:10.5194/acp-10-11471-2010, 2010.

Tan, J., Zhang, L., Zhou, X., Duan, J., Li, Y., Hu, J., and He, K.: Chemical characteristics and source apportionment of PM2.5 in Lanzhou, China, Sci. Total Environ., 601–602, 1743–1752, doi:10.1016/j.scitotenv.2017.06.050, 2017.

Tang, K., Huang, Z., Huang, J., Maki, T., Zhang, S., Shimizu, A., Ma, X., Shi, J., Bi, J., Zhou, T., Wang, G., and Zhang, L.: Characterization of atmospheric bioaerosols along the transport pathway of Asian dust during the Dust-Bioaerosol 2016 campaign, Atmos. Chem. Phys., 18, 7131–7148, doi:10.5194/acp-18-7131-2018, 2018.

Tian, P., Zhang, N., Li, J., Fan, X., Guan, X., Lu, Y., Shi, J., Chang, Y., and Zhang, L.: Potential influence of fine aerosol chemistry on the optical properties in a semi-arid region, Environ. Res., 216, 114678, doi:10.1016/j.envres.2022.114678, 2023.

Tian, P., Liu, D., Bi, K., Huang, M., Wu, Y., Hu, K., Li, R., He, H., Ding, D., Hu, Y., Liu, Q., Zhao, D., Qiu, Y., Kong, S., and Xue, H.: Evidence for anthropogenic organic aerosols contributing to ice nucleation, Geophys. Res. Lett., 49, e2022GL099990, doi:10.1029/2022GL099990, 2022.

Tobo, Y., Uetake, J., Matsui, H., Moteki, N., Uji, Y., Iwamoto, Y., Miura, K., and Misumi, R.: Seasonal trends of atmospheric ice nucleating particles over Tokyo, J. Geophys. Res. Atmos., 125, e2020JD033658, doi:10.1029/2020JD033658, 2020.

Ullrich, R., Hoose, C., Möhler, O., Niemand, M., Wagner, R., Höhler, K., Hiranuma, N., Saathoff, H., and Leisner, T.: A New Ice Nucleation Active Site Parameterization for Desert Dust and Soot, J. Atmos. Sci., 74, 699–717, https://doi.org/10.1175/jas-d16-0074.1, 2017.

Villanueva, D., Stengel, M., Hoose, C., Bruno, O., Jeggle, K., Ansmann, A., and Lohmann, U.: Dust-driven droplet freezing explains cloud-top phase in the Northern Extratropics, Science, 389, 521–525, doi:10.1126/science.adt5354, 2025.

Wagh, S., Singh, P., Ghude, S. D., Safai, P., Prabhakaran, T., and Kumar, P. P.: Study of ice nucleating particles in fog-haze weather at New Delhi, India: a case of polluted environment, Atmos. Res., 259, 105693, doi:10.1016/j.atmosres.2021.105693, 2021.

Wang, M., Tian, P., Wang, L., Yu, Z., Du, T., Chen, Q., Guan, X., Guo, Y., Zhang, M., Tang, C., Chang, Y., Shi, J., Liang, J., Cao, X., and Zhang, L.: High contribution of vehicle emissions to fine particulate pollutions in Lanzhou, Northwest China based on high-resolution online data source appointment, Sci. Total Environ., 798, 149310, doi:10.1016/j.scitotenv.2021.149310, 2021.

Wang, Y., Li, J., Zhao, Y., Li, Y., Zhao, Y., and Wu, X.: Distinct diurnal cycle of supercooled water cloud fraction dominated by dust extinction coefficient, Geophys. Res. Lett., 49, e2021GL097006, doi:10.1029/2021GL097006, 2022.

Wang, Y., Yu, H., Li, L., Li, J., Sun, J., Shi, J., and Li, J.: Long-term trend of dust event duration over northwest China, Sci. Total Environ., 951, 175819, doi:10.1016/j.scitotenv.2024.175819, 2024a.

Wang, Y., Li, J., Fang, F., Zhang, P., He, J., Pöhlker, M. L., Henning, S., Tang, C., Jia, H., Wang, Y., Jian, B., Shi, J., and Huang, J.: In-situ observations reveal weak hygroscopicity in the Southern Tibetan Plateau: implications for aerosol activation and indirect effects, npj Clim. Atmos. Sci., 7, 77, doi:10.1038/s41612-024-00629-x, 2024b.

Wang, Y., Fang, F., Li, J. et al. (2025). High effective supersaturation offsets low aerosol hygroscopicity to promote orographic cloud formation over the southern Tibetan Plateau. npj climate and atmospheric science, 8, 231. doi:10.1038/s41612-025-01119-4

Xu, J., Zhang, Q., Chen, M., Ge, X., Ren, J., and Qin, D.: Chemical composition, sources, and processes of urban aerosols during summertime in Northwest China: insights from high-resolution aerosol mass spectrometry, Atmos. Chem. Phys., 14, 12593–12611, doi:10.5194/acp-14-12593-2014, 2014.

Yakobi-Hancock, J. D., Ladino, L. A., and Abbatt, J. P. D.: Feldspar minerals as efficient deposition ice nuclei, Atmos. Chem. Phys., 13, 11175–11185, doi:10.5194/acp-13-11175-2013, 2013.

Yu, H., Wang, Y., Yuan, L., Kong, R., Han, S., Han, W., and Li, J.: Longer dust events over northwest China from 2015 to 2022, Atmos. Res., 304, 107365, doi:10.1016/j.atmosres.2024.107365, 2024.

Zhang, C., Wu, Z., Chen, J., Chen, J., Tang, L., Zhu, W., Pei, X., Chen, S., Tian, P., Guo, S., Zeng, L., Hu, M., and Kanji, Z. A.: Ice-nucleating particles from multiple aerosol sources in the urban environment of Beijing under mixed-phase cloud conditions, Atmos. Chem. Phys., 22, 7539–7556, doi:10.5194/acp-22-7539-2022, 2022.

Zhao, B., Wang, Y., Gu, Y., Liou, K.-N., Jiang, J. H., Fan, J., Liu, X., Huang, L., Yung, Y. L.: Ice nucleation by aerosols from anthropogenic pollution, Nat. Geosci., 12, 602–607, doi:10.1038/s41561-019-0389-4, 2019.

Zhao, X., Jiang, K., Ou'yang, S., Li, Y., Wang, Y., Wang, J., Zhao, N., and Shen, G.: Global biomass burning emission contributions to ice nucleating particles, Geophys. Res. Lett., 51, e2024GL111881, doi:10.1029/2024GL111881, 2024.